Received: 22 November 2019 | Accepted: 4 September 2021

DOI: 10.1111/jmg.12638

ORIGINAL ARTICLE

Journal of METAMORPHIC GEOLOGY WILEY

Fluid-driven transformation of blueschist to vein eclogite during the Early Eocene in a subducted sliver of continental crust (Monte Emilius, Italian Western Alps)

Sebastian Weber[1,2] | **Matthias Hauke**[3] | **Raul E. Martinez**[1,4] | **Charlotte Redler**[1,5] | **Carsten Münker**[6] | **Nikolaus Froitzheim**[3]

[1]Institute for Earth and Environmental Science, Albert-Ludwigs-University, Freiburg, Germany

[2]Geological Survey of Saxony, Saxon State Agency for Environment, Agriculture and Geology, Freiberg, Germany

[3]Steinmann Institut, University of Bonn, Bonn, Germany

[4]Max-Planck-Research Group Paleobiogeochemistry, University of Bremen, Bremen, Germany

[5]Dezernat Rohstoffgeologie (Mineralogie, Petrologie, Geochemie), Hessisches Landesamt für Naturschutz, Umwelt und Geologie, Wiesbaden, Germany

[6]Institute of Geology and Mineralogy, University of Cologne, Cologne, Germany

Correspondence
Sebastian Weber, Institute for Earth and Environmental Science, Albert-Ludwigs-University, Albertstrasse 23b, D-79104 Freiburg, Germany.
Email: sebastian.weber@smul.sachsen.de

Funding information
Deutsche Forschungsgemeinschaft (DFG), Grant/Award Number: FR700/21-1

Abstract

In the Penninic nappe stack of the Western Alps, high- to ultrahigh-pressure metamorphic ophiolites of the Zermatt-Saas Zone are associated with slivers of continental crust. In one of these slivers, Monte Emilius, the overprinting of pre-Alpine granulite-facies rocks by subduction-related, Alpine eclogite-facies metamorphism can be studied. Mafic granulites were initially transformed into blueschists. In a second step, shear zones were developed in which the blueschists recrystallized to fine-grained, foliated glaucophane eclogites, and eclogite veins. The combination of petrographic and field observations as well as whole-rock compositions suggests that the eclogite assemblage formed only in shear zones where Ca-metasomatism induced a change in major element composition. These substantial differences in bulk rock composition demonstrate how spatially limited eclogitization may be controlled by chemical redistribution, the degree of fabric development, and associated metamorphic reactions along fluid pathways. Thermodynamic modelling of selected bulk rock compositions yielded only slightly different conditions of 1.8 ± 0.1 GPa/550 ± 50°C for blueschist and 1.9–2.3 GPa/550 ± 50°C for eclogite, constraining Ca-rich fluid infiltration and transformation to a depth of ~60–70 km. Eclogitization occurred in the Early Eocene at 52.96 ± 0.91 Ma, as indicated by a well-defined Lu–Hf garnet isochron.

KEYWORDS

eclogite, Lu–Hf garnet geochronology, Monte Emilius, subduction, thermodynamic modelling, Zermatt–Saas zone

1 | INTRODUCTION

Fluids in subduction zones play a key role in tectonic, metamorphic, and magmatic processes at convergent plate boundaries. Fluid availability determines, among other factors, if subduction megathrust faults generate earthquakes or slip aseismically (Bilek & Lay, 2018; Peacock & Hyndman, 1999; Ranero et al., 2008). H_2O and CO_2 enter subduction zones via the subduction of sediments containing hydrous and carbonate minerals and of hydrated and carbonated oceanic crustal rocks like basalt/spilite and serpentinite/ophicalcite

(Peacock, 1990). Fluids leave subduction zones via arc magmas and via upward fluid flow through fractured upper plates and accretionary wedges or along the subduction interface. Some fluids are subducted with the slab to depth and are mixed back into the deeper mantle (Dasgupta & Hirschmann, 2010). Fluid sinks in subduction zones are hydration/alteration of the forearc mantle wedge (Reynard, 2016) and of subducted tracts of fluid undersaturated continental crust.

One source of information about the interplay between metamorphism, deformation, and fluid flow in a subduction zone is the study of exhumed high-pressure (*HP*) terranes in collisional orogens like the Alps. An extensive body of research has demonstrated that eclogites of the Western Alps are the result of subduction during Europe-Adria convergence (Angiboust et al., 2009; Barnicoat & Fry, 1986; Bucher et al., 2005; Ernst, 1988; Ernst & Dal Piaz, 1978; Groppo et al., 2009). In this area, eclogites are found both in ophiolites, representing former Mesozoic oceanic crust (Zermatt-Saas Zone), and in continental basement rocks. The latter include the major nappes Dora-Maira, Gran Paradiso, Monte Rosa, and Sesia, as well as smaller continental slivers lithologically similar to the Sesia Nappe but embedded in ophiolites of the Zermatt-Saas Zone. The largest of these is the Monte Emilius sliver (Ballèvre et al., 1986; Dal Piaz et al., 1983, 2001; Fassmer et al., 2016; Weber et al., 2015; Weber & Bucher, 2015). Whereas oceanic crust releases water during metamorphism in a subduction zone, these continental slivers had previously been "dehydrated" by Permian (Kunz et al., 2018) high-temperature metamorphism. Therefore, they acted as fluid sinks during the *HP* metamorphism. Previous studies have investigated the interplay between fluids and deformation in the tectono-metamorphic evolution of the Monte Emilius sliver under *HP* conditions (Angiboust et al., 2017; Hertgen et al., 2017; Pennacchioni, 1996; Scambelluri et al., 1998, 2017). They discovered eclogitized granulites and eclogite breccias embedded in an eclogitic foliation, dissected by a complex network of eclogite veins. These features preserve evidence for multiple fluid infiltration events leading to extensive chemical mass transfer and to alternating brittle and ductile deformation. In places where mafic boudins and granulites are in contact, fluid–rock interaction processes resulted in the formation of garnetite and clinopyroxenite layers. Samples for this study were taken from a second mafic lithotype, which contains substantial amounts of glaucophane and was defined by Pennacchioni (1996) as type I metabasite. This mafic lithotype represents an interlayered succession of omphacite-free blueschist and intensely foliated eclogite comprising eclogitic veins on a meter scale. Based on whole-rock analyses, petrography, mineral chemistry, and thermodynamic modelling of the eclogites and blueschists, this study proposes that precursor metabasic rocks have undergone prograde conversion from blueschist to eclogite by infiltration of Ca-rich fluid. We also present Lu–Hf isotope data in combination with element mapping for one eclogite sample in order to better constrain the timing of eclogite formation. These data are used to discuss if the transformation of blueschist into eclogite resulted mainly from fluid–rock interaction or from a change in the *P–T* conditions, and during which time interval it took place.

2 | GEOLOGIC SETTING

The nappe stack of the internal Swiss-Italian Western Alps developed during the Alpine orogeny from Late Cretaceous to Paleogene time (Oberhänsli & Goffé, 2004; Steck et al., 2015). The palaeogeographical realm of the Western Alps was heterogeneous, formed partly by continental crust, partly by oceanic crust of mainly Jurassic (Rubatto et al., 1998) and subordinately Cretaceous age (Liati & Froitzheim, 2006). Today, the remnants of the palaeogeographical Western Alpine domain are preserved as continental slivers and Penninic ophiolites. For a detailed description of the palaeogeographical relationships, prior to Late Cretaceous–Cenozoic convergence, the reader is referred to previous studies (Pleuger et al., 2007; Rosenbaum & Lister, 2005; Schmid et al., 2004; Stampfli et al., 1998).

2.1 | Penninic ophiolites

The Penninic ophiolites in the internal Western Alps are classically divided into two principal units, the Combin Zone and the Zermatt-Saas Zone (ZSZ; Ballèvre & Merle, 1993; Dal Piaz et al., 2001; Bousquet et al., 2004; Angiboust et al., 2014; Figure 1). The Combin Zone is further subdivided into the oceanic-crust derived Tsaté Nappe and the continent-derived metasediments of the Cimes Blanches and Frilihorn nappes (Escher et al., 1997). Within the ophiolites of the ZSZ the record of *HP* to ultra-high-pressure (*UHP*) metamorphism is well preserved. It is assumed to result from subduction towards southeast under the Adriatic continental margin (Barnicoat & Fry, 1986). Peak metamorphic conditions were in the range of 2.4–3.0 GPa/550°C–650°C (Angiboust et al., 2009; Bucher et al., 2005; Groppo et al., 2009; Rebay et al., 2012). The occurrence of coesite and diamond at one locality in the ZSZ, Lago di Cignana, indicates *UHP* metamorphism (Reinecke, 1991). Ages for the eclogite-facies metamorphism are predominantly between ~50 and ~40 Ma, decreasing from higher to

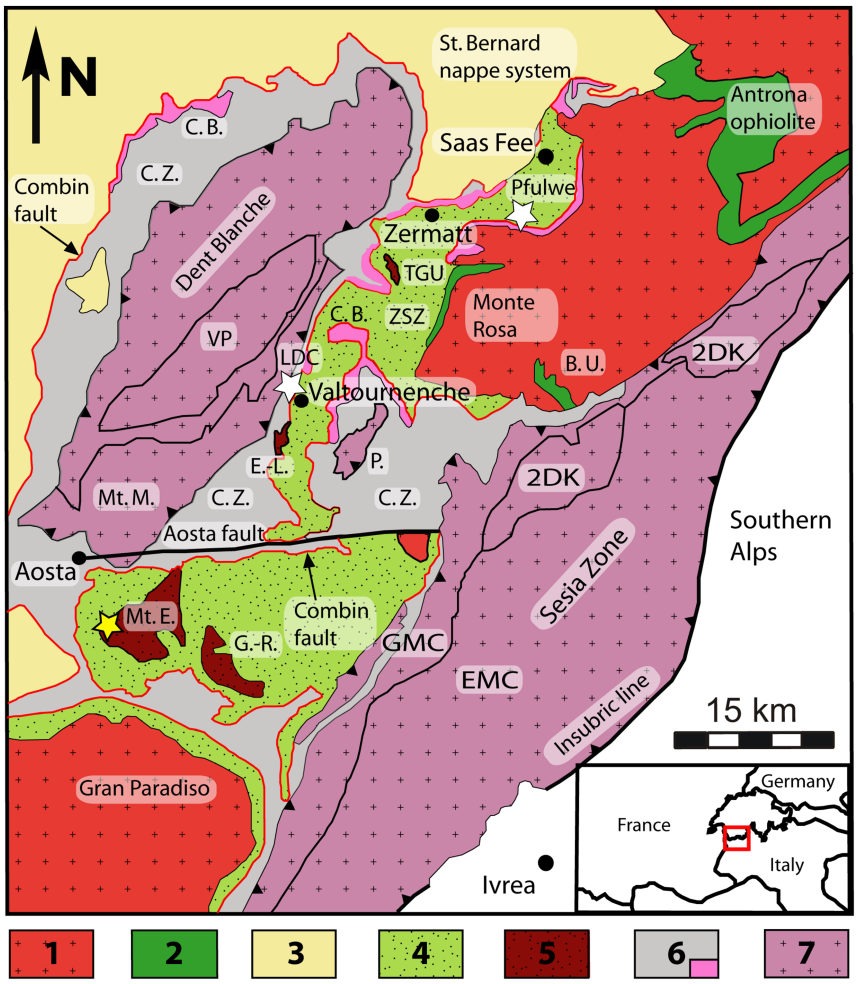

FIGURE 1 Tectonic map of the northwestern Alps (modified after Dal Piaz et al., 1981). Yellow star indicates the location of the area studied in this work and the white stars indicate the location of the Lago di Cignana and the Pfulwe pass areas, respectively. The red line represents the Combin fault, which separates the Combin zone from the underlying ZSZ and the St. Bernard nappe system. Although the Tsate nappe and the Cimes Blanches are considered as derived from the greenschist to blueschist facies South Penninic ophiolites, they are designated as a separate unit. Lithologic patterns: (1) Internal Crystalline Massifs (Sub-Penninic), (2) North Penninic ophiolites (Lower-Penninic), (3) Briançonnais (middle-Penninic), (4) Eclogitic facies South Penninic ophiolites (Upper-Penninic), (5) continental outliers (Austroalpine or Upper-Penninic), (6) Greenschist to blueschist facies south Penninic ophiolites (Combin Zone + Cimes Blanches), (7) Sesia-Dent Blanche nappe system (Austroalpine or Upper-Penninic). Abbreviations: B.U. = Balma unit, 2DK = Seconda Zona Dioritico-Kinzigitica, GMC = Gneiss Minuti complex, EMC = Eclogitic Micaschist complex, TGU = Theodul Glacier Unit, LDC = Lago di Cignana, P. = Pillonet klippe, C.B. = Cimes Blanches, E.-L. = Etirol-Levaz slice, M.E. = Mount Emilius, G.-R. = Glacier Refray, Mt.M. = Mount Mary, VP = Valpelline, C.Z. = Combin Zone, ZSZ = Zermatt-Saas Zone [Colour figure can be viewed at wileyonlinelibrary.com]

lower structural levels (Rubatto et al., 1998; Skora et al., 2015). Recently, *HP* ages of ~65 Ma have been proposed for a portion of the ZSZ (Rebay et al., 2018). There is little information on the *HP* evolution of the Combin Zone, due to the scarcity of diagnostic minerals such as garnet (Angiboust et al., 2014; Bousquet et al., 2004; Reddy et al., 1999). Recent studies have reported conditions of 0.7–1.5 GPa/360°C–530°C for the Combin Zone (Angiboust et al., 2014; Negro et al., 2013).

North of the Aosta Fault (Figure 1), the Combin Zone generally lies on top of the Zermatt-Saas Zone and the latter lies on the Europe-derived continental basement of the Monte Rosa Nappe. South of the Aosta Fault, the situation is different. Here, the structurally lowest unit is the continental Gran Paradiso Nappe, equivalent to the Monte Rosa Nappe. It is overlain at its northern border first by a mélange including Zermatt-Saas-type, eclogite-facies ophiolites. Above are blueschist-facies calcschists and ophiolites of Combin type, in turn overlain by Zermatt-Saas-type eclogite-facies meta-ophiolites (Ellero & Loprieno, 2018). This situation is probably caused by a large-scale, northwest-southeast trending, recumbent synformal fold with the Combin rocks in the core (Ellero & Loprieno, 2018). The uppermost unit of

the nappe stack is the continent-derived Sesia Nappe. Characteristic features of the Sesia Nappe are Permian-age bimodal magmatism and high-temperature metamorphism (Engi et al., 2018; Kunz et al., 2018) and Late Cretaceous *HP* metamorphism of eclogite-facies (~75 to 65 Ma; Rubatto et al., 1999). North of the Aosta Fault, the large klippe of the Dent Blanche Nappe represents a noneclogitic outlier of the same nappe, isolated from the rest by erosion through an antiformal hinge.

2.2 | Continental slivers

Monte Emilius belongs to a group of continental slivers lithologically similar to the Dent Blanche-Sesia Nappe (Ballèvre et al., 1986), including the Etirol-Levaz slice (Dal Piaz et al., 2001 and references therein; Fassmer et al., 2016), the Theodul Glacier Unit (Weber et al., 2015; Weber & Bucher, 2015), the Glacier-Rafray Unit and other minor basement slices (Figure 1). These slivers have been termed "Austroalpine outliers," "Continental outliers" (Dal Piaz et al., 2001), or "Sesia-type basement slivers" (Pleuger et al., 2007). They occur both north and south of the Aosta Fault. North of the fault, the slivers lie at the top of the Zermatt-Saas Zone (Etirol-Levaz Unit) or within the upper part of it (Theodul Glacier Unit). The slivers consist of continental basement rocks, devoid of Mesozoic cover, with Permian-age (Bucher et al., 2020; Kunz et al., 2018) high-temperature metamorphism (Bucher et al., 2019), overprinted by Palaeocene to Eocene eclogite-facies metamorphism (Dal Piaz et al., 2001; Fassmer et al., 2016; Weber et al., 2015). The Theodul Glacier Unit has recently been reconsidered as a sedimentary sequence deposited on the oceanic crust of the ZSZ ophiolite (Bovay et al., 2021).

The Monte Emilius tectonic klippe forms some high peaks towering above the Aosta Valley, culminating in Monte Emilius itself (3559 m). On all sides, the basement sliver rests with a tectonic contact on eclogite-facies ophiolites of Zermatt-Saas type. The Mt. Emilius sliver has a composite internal structure comprising voluminous gneisses and micaschists with subordinate interbedded layers of eclogite, serpentinite, and marble (Dal Piaz et al., 1983). It preserves a polymetamorphic history of (1) pre-Alpine mineral relics of granulite to amphibolite-facies (Benciolini, 1996; Dal Piaz et al., 1983; Pennacchioni, 1996), (2) a pervasive Alpine *HP* metamorphic overprint (Angiboust et al., 2017; Compagnoni, 1977), and (3) a decompression-related mineral assemblage, which formed progressively under blueschist- to greenschist-facies conditions (Dal Piaz et al., 1983). Radiometric results for inferring the timing of eclogitic imprint in the Monte Emilius sliver are restricted to Rb–Sr phengite ages of 49–40 Ma (Dal Piaz et al., 2001). Since the rocks of the Mt. Emilius sliver are similar in many respects to those found within the Eclogitic Micaschist Complex of the Sesia Nappe, for example, recording both granulite-facies relics and eclogite-facies overprint, they are generally interpreted to be closely related to the Sesia-Dent-Blache nappe system (Compagnoni, 1977; Dal Piaz et al., 1983; Gosso et al., 2010; Lardeaux & Spalla, 1991). Alpine peak conditions for the eclogites of Monte Emilius have been estimated at 2.1–2.4 GPa /500°C–550°C (Angiboust et al., 2017). These results are similar to *P–T* conditions for eclogites from the Etirol-Levaz slice, 2.0–2.5 GPa/660°C, and from the Theodul Glacier Unit, 2.2 ± 0.1 GPa/580 ± 65°C (Fassmer et al., 2016; Weber & Bucher, 2015).

3 | METHODS

Twenty-four samples were collected for this study, focusing on a large, coherent body of metabasite (Figure 2). After thin section examination, 10 samples were chosen for a detailed study. Bulk rock compositions were acquired using an X-ray fluorescence Philips 2404 instrument operating at different voltage (kV) and current (mA) levels for each element measured. Fused beads were used for major elements, and powder pellets for trace elements. All mineral analyses were done using a CAMECA SX 100 electronprobe microanalyzer. Elements were determined at 15 kV and 20 nA beam current with a focused electron beam with peak counting times at 20 s. For feldspar and mica minerals 10 kV was used, because alkaline elements show a high sensitivity to high accelerating voltage. Natural oxide and silicate standards were used for calibration. Both instruments are located at the Institute of Mineralogy and Geochemistry in Freiburg.

For Lu–Hf dating, sample SW108 was chosen. The sample was crushed in a steel mortar and further processed with a steel disc mill. One split of the crushed sample was ground to powder with an agate ball mill. The other split was sieved into several grain sizes. For mineral separation a vibrating table and a FRANZ® magnetic separator were used. The final garnet separates were handpicked under a binocular microscope from the 250–500 μm and from the 500–1000 μm split. Prior to the dissolution the garnet separates were cleaned in 3 M HCl for about 5 min and rinsed several times with MQ® water to remove possible surface contaminations. To all separates a 176Lu–180Hf spike was added. The garnet separates and two whole-rock separates were dissolved via the "tabletop" digestion after Lagos et al. (2007). This

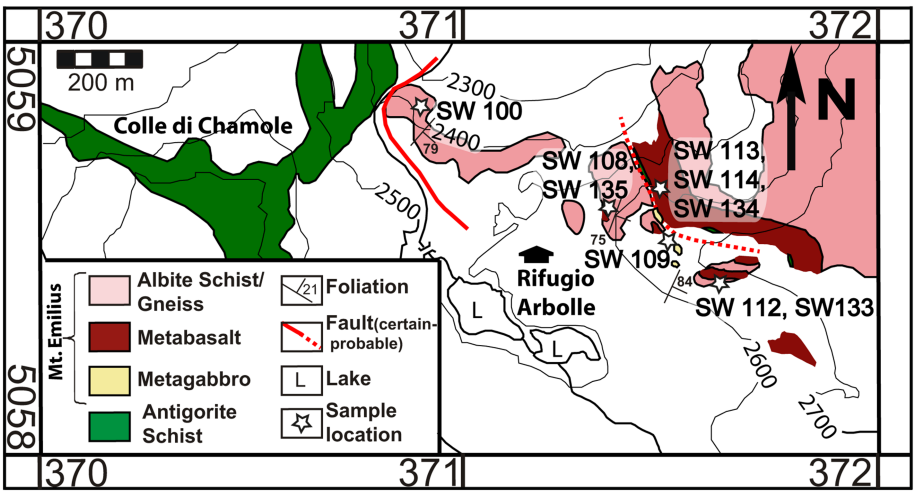

FIGURE 2 Geological map of the sample locality near the Rifugio di Arbolle. Note that sample locations are highlighted as white stars. The figure is modified after Pennacchioni (1996) and Scambelluri et al. (1998). The UTM (WGS 84) coordinate system is used for reference [Colour figure can be viewed at wileyonlinelibrary.com]

method leaves behind Hf-rich phases like zircon and rutile, which might preserve unequilibrated isotope signatures. To achieve this selective digestion a mixture of HF, HNO_3 and $HClO_4$ (4:2:1) was used. First the separates remained with the HF, HNO_3 mixture in closed Savilex® vials at 120°C on a hotplate for 48 h. Before the evaporation of the HF, HNO_3 mixture the $HClO_4$ was added, which was evaporated at higher temperatures afterwards. After the evaporation the separates were dissolved in 6 N HCl. If this solution was cloudy or undissolved garnet grains were visible the procedure was repeated until a clear solution with only the eventually remaining rutiles and zircons was achieved. To also dissolve zircon and rutile two spiked whole-rock separates were digested for 4 days in a mixture of HF and HNO_3 (1:1) in a Savilex® vial inside PARR® steel bombs at 180°C using MQ® water as an outer pressure medium. Lu and Hf were separated via the column chemistry method of Münker et al. (2001) extended by the clean-up step after Lagos et al. (2007). To further eliminate the interferences of 176Lu and 176Yb on the 176Hf the clean-up step after Lagos et al. (2007) was repeated a second time.

The measurements were performed at the Institute of Geology and Mineralogy at the University of Cologne with a Thermo Scientific® Multicollector ICP-MS. Isobaric interferences on 176Hf and 180Hf were corrected by monitoring 173Yb, 175Lu, 181Ta, and 183 W. Mass bias was corrected using the exponential law and a 179Hf/177Hf of 0.7325. All 176Hf/177Hf are given relatively to the Münster Ames standard (176Hf/177Hf = 0.282160), which is indistinguishable from the JMC-475 standard (Münker et al., 2001). Hf compositions were calculated with the tracers and natural Lu compositions and the difference was added to the external reproducibilities. The external reproducibilities were estimated following the general approach of Bizzarro et al. (2003). For Lu measurements isobaric interferences were corrected by the measurement of 173Yb and 177Hf and their measured isotopic composition. Lu isotope ratios were corrected for mass bias by naturally occurring Yb in the Lu cuts (Vervoort et al., 2004). Procedural blanks for garnet and tabletop whole-rock separates were between 30 and 82 pg for Hf and between 2 and 181 pg for Lu. Procedural blanks for the bombed whole rocks were <328 pg Hf and <97 pg Lu. Ages were calculated with Isoplot v. 4.1 (Ludwig, 2008) and a 176Lu decay constant of 1.867×10^{-11} $year^{-1}$ (Scherer et al., 2001, 2003; Söderlund et al., 2004).

4 | FIELD OCCURRENCE

The metabasites investigated in this study were sampled from the Arbolle area, located along the northwestern part of the Mt. Emilius sliver, which has been mapped in detail previously (Pennacchioni, 1996; Scambelluri et al., 1998; Figure 2). The sampling area is accessible from Pila and is located close to Rifugio Arbolle (Figure 3a). The western part of the map in Figure 2 shows the ophiolites underlying the basement sliver. These consist mainly of antigorite schist, a characteristic lithotype of the ZSZ (Figure 2). The ophiolitic rocks are separated from the continental Mt. Emilius sliver by a major tectonic contact. The most widespread lithotypes are albite gneisses and schists, which locally preserve evidence of *HP* metamorphism (Pennacchioni, 1996; Scambelluri et al., 1998). On the macroscopic scale, these gneisses show centimetre-sized augen-like feldspar blasts, quartz, and greenish-black amphiboles (Figure 3b). Most rock types have been affected by an intense penetrative metamorphic and structural reworking under eclogite-facies conditions. This led to the formation of the main

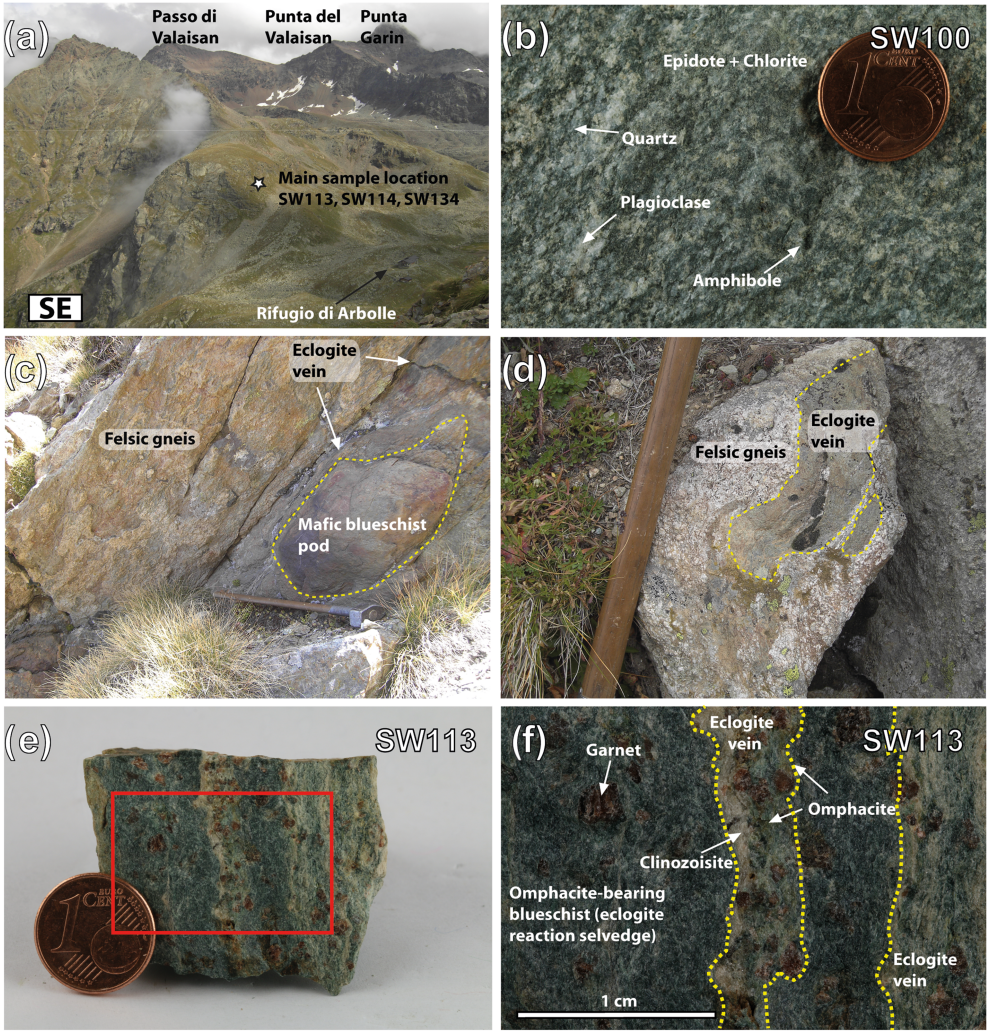

FIGURE 3 (a) Overview of the main sample location of this study. The white star shows the main sample location near the Rifugio di Arbolle shown for scale. (b) Felsic-gneisses (albite-gneisses) revealing centimetre-sized augen-like feldspar blasts and greenish-black amphiboles. (c) Field photograph of adjacent eclogite veins and blueschist pods. (d) Field photograph of eclogite vein crosscut surrounding felsic gneisses. (e,f) Reaction halos of omphacite-bearing blueschists (in the following referred to as foliated glaucophane eclogite) along eclogite-veins with rather sharp boundaries. Note that the transitional boundaries between the foliated glaucophane eclogites and the omphacite-free blueschists have not been recognized at the outcrop scale [Colour figure can be viewed at wileyonlinelibrary.com]

regional schistosity that predominantly strikes NW–SE. In this area, the first and second deformation phases (D_1 and D_2) occurred under *HP* conditions while the third deformation phase (D_3) was related to the retrograde greenschist-facies overprint (Dal Piaz et al., 1983; Pennacchioni, 1996).

In the eastern parts of the map (Figure 2), the felsic gneisses are interbedded with metabasite (Figure 3c). The main body of these mafic rocks is represented by an elongate NW-SE trending layer, extending almost one kilometre in length, as described previously (Pennacchioni, 1996; Scambelluri et al., 1998). It was mapped as eclogitized granulite by Pennacchioni (1996). Within this body, a set of pale-green eclogite veins occurs within and along discrete pods or layers of more massive, dark-bluish-grey blueschist (Figure 3c). These eclogite veins not only crosscut mafic blueschist pods but also the felsic gneiss country rock (Figure 3d). Blueschist intimately associated with the eclogite veins shows light green reaction selvedges caused by omphacitization (see Pennacchioni, 1996; Figure 3e,f), whereas this feature is absent in blueschist lacking eclogite veins. The vein thicknesses range from millimetres to several centimetres, with sharp boundaries towards the blueschist and felsic gneiss. The size and diameter vary along individual veins, occasionally with anastomosing and branching forms. Eclogite veins in most cases follow the orientation of the prevailing regional foliation. However, in some cases, oblique veins are observed. The interface between the eclogite veins and the adjacent blueschists appear to be concordant to the metamorphic layering, which may be a compositional heterogeneity from the protolith or an Alpine foliation or both. Garnet porphyroblasts are present in both the blueschist pods and inside the eclogite veins. The large metabasite layer is separated from the underlying gneisses by a basal tectonic contact, marked by thin slices of serpentinite. In addition, meter-sized bodies of metagabbro are found in close vicinity of the tectonic contact. These metagabbros likely represent Permian mafic intrusives, as are frequently found in the Sesia-Dent Blanche nappe system (Manzotti et al., 2017).

5 | MICROSTRUCTURAL RELATIONSHIPS AND MINERAL COMPOSITION OF THE ECLOGITE VEINS AND BLUESCHISTS

Within the vein-host-rock system of the Arbolle area, blueschists and eclogite veins can be distinguished based on their *HP* mineral content. The major rock forming minerals occur in different proportions but the assemblages are the same for all lithotypes (Table 1). Blueschist is composed of garnet + colourless blocky glaucophane + tabular clinozoisite + fibrous sheaf-like chlorite aggregates + poorly oriented white mica flakes + quartz. It is generally equigranular (grain diameter is 0.1 to 2 mm), consists of rather optically-stress free crystals, is marked by a weak Alpine alignment along the foliation plane and by a lack of omphacite. By contrast, eclogitic veins crosscutting the blueschists are relatively coarse-grained (grain diameter is 0.1 to 1 mm), glaucophane-free, and composed of garnet + omphacite + clinozoisite + quartz. Within the eclogite veins, omphacite shows shape-preferred alignment parallel to the orientation of the foliation outside the vein. Finally, the contact between blueschists and eclogitic veins is characterized by green reaction selvedges. These are mostly medium- to fine-grained (grain diameter is 0.1 to <0.01 mm) and consist of garnet + omphacite + glaucophane + clinozoisite + quartz. This assemblage shows a well-defined grain-shaped preferred orientation for omphacite, glaucophane and clinozoisite crystals, which is probably best interpreted as a *HP* foliation. The main foliation curves around garnet porphyroblasts, such that the matrix foliation is not continuous with the spiral-shaped inclusion trails inside individual garnet crystals. This shows that garnet preserves an older internal foliation. The presence of omphacite which, together with glaucophane, defines a plano-linear fabric indicates that these blueschists have developed an eclogitic foliation and therefore should be considered as glaucophane-bearing eclogite (in the following referred to as foliated glaucophane eclogite).

5.1 | *HP* assemblage of the eclogites and blueschists

5.1.1 | Garnet

Garnet blasts are abundant in blueschists and foliated glaucophane eclogites as well as in the eclogite veins. Even though intermediate sized crystals occur, a bimodal grain size distribution can be clearly defined. The first generation of garnet (Grt1) is present in blueschist and foliated glaucophane eclogite, is more subhedral and coarser-grained (up to 5 mm in diameter), and contains inclusions of glaucophane, omphacite, Ca-rich amphibole, clinozoisite, titanite, apatite, and quartz (Figure 4a). Omphacite inclusions are only present in the rims of Grt1 within foliated glaucophane eclogites, typically in close proximity to eclogite veins (Figure 5a).

TABLE 1 Mineral assemblages present in Arbolle metamafics

Sample no.	SW108a	SW111a	SW113a	SW114a	SW115a	SW133a	SW134a	SW135a	SW109b	SW112b
Location	**E**	**E**	**E**	**E**	**E**	**B**	**B**	**B**		
Grt	xV	xV	xV	xV	xV	x	x	x		
Omp/Cpx	xV	xV	xV	xV	xV					
WM						x	x	x	(x)	
Gln	x	x	x	x	x	x	x	x		
Pl/Alb	xS	xS	xS	xS	xS	xS	xS	xS	x	x
Cam	xS	xS	xS	xS	xS	xS	xS	xS	x	x
Ep/Czo	xV	xV	xV	xV	xV	x	x	x	x	x
Chl	(x)	(x)	(x)			xS	xS	xS		
Tit	x	x	x	x	x	x	x	x		
Qtz	xV	xV	xV	xV	xV	x	x	x	(x)	(x)
Other	Ap, Cal	Ap, Opq	Ap, Cal	Ap, Cal	Ap, Cal	Ap, Opq	Ap, Cal	Ap, Cal	Opq	Ap, Opq
	Opq		Opq	Opq	Opq		Opq	Opq		

Note: V = occurs as mineral vein; S = occurs in breakdown symplectite around HP phases; x = essential mineral; (x) = mineral only present in small amounts, Grt = garnet, Omp = omphacite, Cpx = clinopyroxene, WM = white mica, Pl = plagioclase, Alb = albite, Ep = epidote, Czo = clinozoisite, Gln = glaucophane, Cam = Ca-clinoamphibole, Chl = chlorite, Tit = titanite, Qtz = quartz, Ap = apatite, Cal = calcite, Opq = opaque phase. E = eclogite veins + foliated glaucophane eclogites, B = blueschist, a metabasalt, b metagabbro.

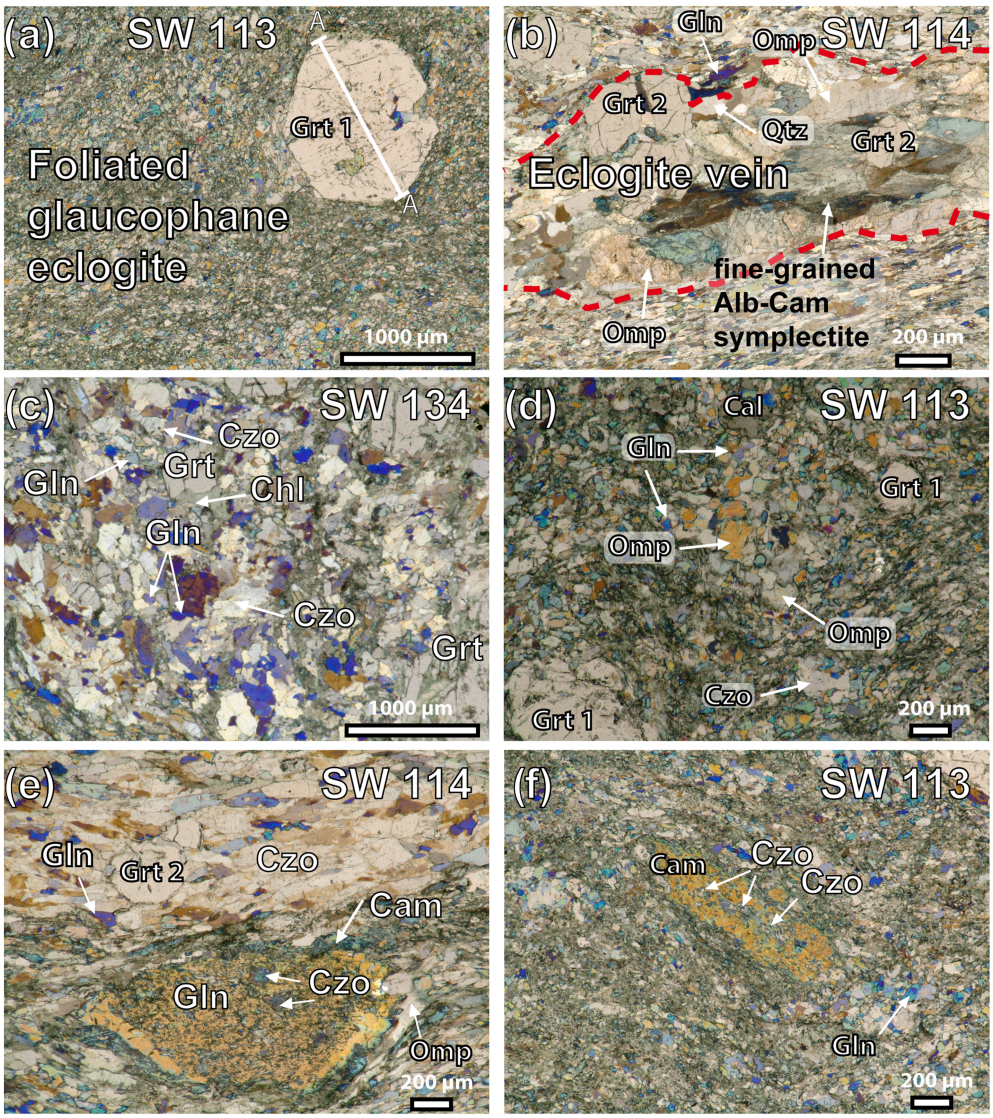

FIGURE 4 Representative photomicrographs of Arbolle metabasalts as seen under optical microscope using plane polarized light: (a) Grt1 porphyroblast embedded in the foliated glaucophane eclogites. A–A` shows a profile trace of compositional cross section of garnet shown in Figure 8e. (b) Vein-forming omphacite showing undulose extinction associated with Grt2, Czo, and Qtz. Note the sharp interfaces between the eclogite-vein and the surrounding high-strain volumes of the foliated glaucophane eclogites. (c) Omphacite-free, low strain blueschist, where the mineral assemblage of Omp + Grt2 does not develop. (d) Mostly medium to fine-grained, high-strain volume of the foliated glaucophane eclogites. (e) Large amphibole blast completely transformed to glaucophane during the Alpine metamorphism. Note the inclusion-free rims. (f) Large glaucophane blast replaced by Ca-rich amphibole [Colour figure can be viewed at wileyonlinelibrary.com]

A second garnet grain population (Grt2) is more euhedral and generally smaller (0.05–1 mm in diameter) than Grt1. It occurs in the eclogite veins and is absent in the surrounding blueschist (Figures 4b and 5b,c). Inclusions are far less common in Grt2. The two populations of garnet can also be distinguished on the basis of compositional zoning patterns. Grt1 rim compositions are in the range of $Alm_{56–60}$ $Grs_{26–30}$ $Py_{6–10}$ $Sps_{0.5–3}$ and core compositions in the range of $Alm_{49–55}$ $Grs_{30–32}$ $Py_{4–6}$ $Sps_{4–12}$ (Figure 6a; Table 2). X-ray mapping indicates prograde zoning in Grt1 cores and multiple chemical oscillations of minor amplitude for spessartine component in Grt1 rims (Figure 7). Grt1 porphyroblasts in both eclogite and blueschist thus display a prograde zoning pattern (Figure 8d,e), which is partly overprinted by diffusional relaxation leading to flattening of compositional zoning patterns. In cases where a prograde zoning is preserved, almandine component is always negatively correlated with spessartine component from the core to the rim. Pyrope component progressively increases towards the rim, while spessartine is strongly enriched in the core. The calculated amount of andradite component is negligible. Grt2 displays a weaker or absent prograde zoning pattern (Figure 8f) but compositions of individual porphyroblasts are more variable in the range of $Alm_{50–57}$ $Grs_{30–35}$ $Py_{4–9}$ $Sps_{1–10}$. Thus, the compositional variations may indicate that idiomorphic, compositionally diverse Grt2 grains formed at the expense of pre-existing, zoned Grt1, depending on whether or not Grt2 consumed Grt1 core or rim material.

5.1.2 | Omphacite

Omphacite occurs in coarse-grained eclogite veins, which are mostly parallel to the foliation in the surrounding reaction selvedge (Figures 4b and 5b,d). Occasionally, these veins crosscut the foliation. Omphacite grains show

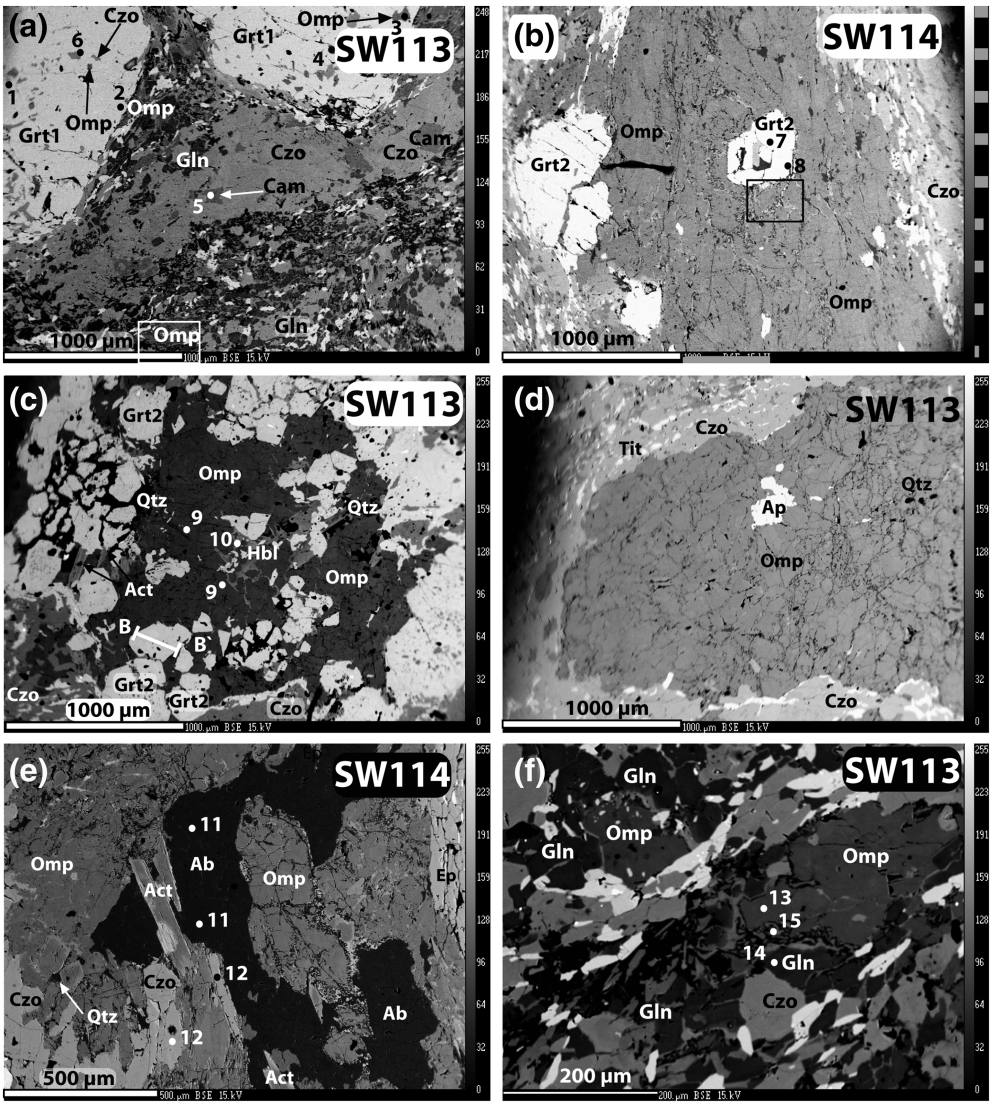

FIGURE 5 Backscattered electron images of selected microstructural domains of the eclogite-veins and adjacent foliated glaucophane eclogites investigated by EMPA: (a) Omphacite inclusion within Grt1. The box represents the position of Figure 5f. (b) Typical omphacite-dominated mineral-vein associated with Grt2, Czo, and Qtz. Note that clinozoisite is localized along the vein walls. The box represents the position of Figure 8a. (c) Eclogite-vein associated with Grt2, Qtz and intergrowths of actinolite. B–B` shows the profile trace of the compositional cross section of garnet shown in Figure 8f. (d) Eclogite-vein associated with Qtz and accessory apatite and without any Grt2. (e) Albite vein crosscutting the eclogite-veins. Note that only locally thin reactions rim textures between omphacite and albite have been developed. (f) Equilibrium texture between Omp and Gln + Cz + Qtz in the high-strain transition zones surrounded by reactions rims. The dots show the exact spatial location of analysed spots: (1) Grt1, texture 1, Table 2, (2) Grt1, texture 2, Table 2, (3) Omp, texture 3, Table 3, (4) Act, texture 5, Table 5, (5) Act, texture 10, Table 5, (6) Czo, texture 5, Table 6, (7) Grt2, texture 3, Table 2, (8) Grt2, texture 4, Table 2, (9) Omp, texture 2, Table 3, (10) Hbl, texture 7, Table 5, (11) Pl, texture 1, Table 6, (12) Czo, texture 4, Table 6, (13) Omp, texture 1, Table 3, (14) Gln, texture 1, Table 5, (15) Act, texture 8, Table 5

elongated habit and interlobate boundaries (Figure 4b). The majority of vein omphacite shows undulose extinction and subgrain boundaries, indicating plastic deformation. The grains show a shape-preferred orientation along the foliation plane. Vein omphacite is intimately associated with euhedral Grt2 + clinozoisite + quartz ± apatite and surrounded by symplectites of albite + Ca-rich amphibole (Figure 5c,e). However, depending on the different mineral contents, several types of veins can be observed. Within the most common veins, Grt2 and clinozoisite are preferentially located along the vein walls, while other veins lack Grt2. Vein omphacite is almost devoid of mineral inclusions. However, in some cases small inclusions of quartz can be found.

The transition from eclogite veins to the surrounding foliated glaucophane eclogite is rather sharp (Figures 4b and 5b). Relatively anhedral omphacite blasts occur in

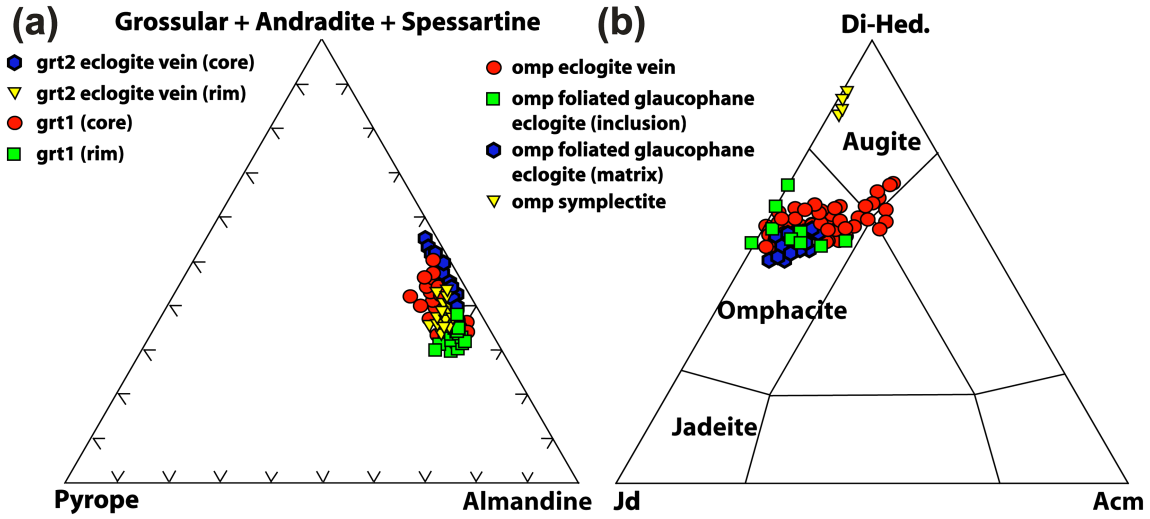

FIGURE 6 (a) Garnet compositions for core and rim analyses associated to eclogite-veins, foliated glaucophane eclogites and adjacent blueschist listed in Table 2. (b) Omphacite compositions listed in Table 3 [Colour figure can be viewed at wileyonlinelibrary.com]

close proximity to the eclogite veins inside the foliated glaucophane eclogite (Table 3; Figures 5f and 9a). Similar to omphacite in the veins, omphacite of the foliated glaucophane eclogite is aligned parallel to the foliation and shows undulose extinction. In these domains, matrix omphacite grains are in contact with glaucophane, clinozoisite, and titanite with no intergranular reactions rims (Figure 9b). Omphacite in veins shows higher diopside + hedenbergite content compared with omphacite blasts in the surrounding rock, which are enriched in jadeite ($Jd_{20–45}$ $Di\text{-}Hed_{50–60}$ $Ac_{0–22}$; Table 3; Figures 5c and 6b). In all cases, omphacite exhibits a weakly developed and non-systematic zoning pattern.

5.1.3 | White mica

Blueschist contains phengite and paragonite. Phengite occurs in abundant amounts throughout the blueschist matrix and shows no preferred orientation. Paragonite is very rare (Table 4; Figure 9c). Neither phengite nor paragonite were detected in eclogitic domains. Si^{4+} in phengite ranges from 3.3 to 3.4.

5.1.4 | Amphibole

Glaucophane is the prevailing *HP* amphibole. It is very commonly found in the groundmass of foliated glaucophane eclogites and blueschists but is lacking in eclogite veins. In blueschist, glaucophane often forms clusters of rather undeformed, equant blasts (Figures 4c and 9d). In foliated glaucophane eclogites, elongate, bulky glaucophane needles define a plano-linear fabric (Figure 9e). Mostly straight grain boundaries between glaucophane and omphacite indicate textural equilibrium in the foliated glaucophane eclogites (Figures 4d and 9a). Rarely, large glaucophane crystals contain abundant inclusions of Ca-rich amphibole, epidote and titanite. These glaucophane crystals have probably replaced pre-Alpine amphibole (Figure 4e,f; Dal Piaz et al., 1983). Glaucophane is always nearly pure end-member glaucophane with only a minor amount of Ca (Figure 10) and shows only slight compositional variations (Table 5). Besides glaucophane, actinolite locally occurs in the foliated glaucophane eclogites in pressure shadows around Grt1 in textural equilibrium with omphacite, glaucophane, clinozoisite and quartz. Thus, it can be assumed that an actinolite-rich amphibole may have been stable at least during some parts of the *HP* stage (Figure 9f).

5.1.5 | Other phases

Quartz is present within both blueschist and eclogite. The spatial association of quartz with omphacite indicates its presence during peak pressure (Figures 4b and 5c,e). In addition to quartz, coarse-grained clinozoisite is an abundant mineral in the eclogite vein assemblage (Table 6; Figure 5b,e). Clinozoisite in veins shows a prismatic habitus and yields an average X_{Fe} of 0.16–0.19. Tiny rutile inclusions between 1 and 10 μm are concentrated in titanite. The occurrence of titanite in the peak assemblage, rather than rutile, may be explained by the unusually Ca-rich bulk composition (Gao et al., 2007; Gao &

TABLE 2 Representative garnet composition of the Arbolle metabasite

Sample no.	SW113				SW114				SW134	
Mineral	Grt 1	Grt 1	Grt 2	Grt 2	Grt 1	Grt1	Grt 2	Grt 2	Grt 1	Grt 1
Texture	1	2	3	4	1	2	3	4	1	2
SiO_2 (wt%)	38.18	38.23	37.91	38.06	38.25	38.61	37.95	38.50	37.76	38.36
TiO_2	0.13	0.28	0.22	0.06	0.23	0.09	0.21	0.03	0.11	0.06
Al_2O_3	21.17	21.35	21.01	20.97	21.02	21.14	21.15	21.57	21.50	21.73
Cr_2O_3	0.02	0.04	0.08	0.13	0.04	0.05	0.04	0.00	0.00	0.11
FeO	27.05	27.80	24.51	27.12	23.64	29.01	22.90	27.58	28.91	27.67
MnO	2.53	0.34	4.30	0.52	6.06	0.37	6.11	0.45	1.35	0.32
MgO	1.31	2.39	0.81	1.49	0.99	2.29	0.74	2.41	1.63	2.49
CaO	11.71	11.46	12.65	13.04	11.71	11.26	12.80	11.78	10.99	11.62
Total	102.12	101.91	101.51	101.40	101.98	102.82	101.89	102.32	102.28	102.38
Si^{4+} (apfu)	2.98	2.97	2.98	2.98	2.99	2.98	2.97	2.97	2.94	2.96
Ti^{4+}	0.01	0.02	0.01	0.00	0.01	0.01	0.01	0.00	0.01	0.00
Al^{3+}	1.95	1.95	1.95	1.93	1.94	1.92	1.95	1.96	1.97	1.98
Cr^{3+}	0.00	0.00	0.01	0.01	0.00	0.00	0.00	0.00	0.00	0.01
Fe^{3+}[a]	0.08	0.07	0.07	0.10	0.04	0.11	0.08	0.09	0.13	0.09
Fe^{2+}	1.69	1.73	1.55	1.70	1.51	1.77	1.42	1.69	1.75	1.70
Mn^{2+}	0.17	0.02	0.29	0.03	0.40	0.02	0.41	0.03	0.09	0.02
Mg^{2+}	0.15	0.28	0.10	0.17	0.12	0.26	0.09	0.28	0.19	0.29
Ca^{2+}	0.98	0.95	1.07	1.09	0.98	0.93	1.07	0.98	0.92	0.96
SUM	8.00	8.00	8.00	8.00	8.00	8.00	8.00	8.00	8.00	8.00
Almandine	56.52	58.04	51.67	56.35	50.15	59.17	47.54	56.92	59.44	57.21
Pyrope	5.10	9.27	3.17	5.83	3.84	8.83	2.90	9.33	6.42	9.66
Grossular	31.39	30.51	34.15	34.77	31.75	29.44	34.30	31.33	28.09	30.86
Spessartine	5.60	0.75	9.57	1.16	13.36	0.81	13.58	0.99	3.02	0.71
Andradite	1.24	1.14	1.14	1.70	0.64	1.62	1.43	1.40	1.93	1.41

Note: Totals include traces of Na and K.
[a]Fe^{3+} contents were calculated by oxide charge balance. The calculated andradite content is mean. (1) core composition of Grt 1 present in foliated glaucophane eclogite and blueschist; (2) rim composition of Grt 1 present in foliated glaucophane eclogite and blueschist; (3) core composition of Grt 2 associated with eclogite-veins; (4) rim composition of Grt 2 associated with eclogite-veins.

Klemd, 2001; Zack & John, 2007). Accessory apatite is present in both blueschist and eclogite. No coesite or other evidence of *UHP* metamorphism was found in the Arbolle metabasites.

5.2 | Retrograde assemblage of the eclogites and blueschists

5.2.1 | Albite

Fine-grained symplectites of albite and actinolite replace omphacite along the rims (Table 6; Figures 5f and 8a). Additionally, in some places fibrous albite veinlets cut obliquely across the blueschist and the eclogite (Table 6; Figure 5e). In contact with omphacite, these albite veins show no or very thin symplectite rims. Albite constitutes part of the retrograde greenschist-facies assemblage together with epidote, actinolite and chlorite.

5.2.2 | Amphibole

Retrograde amphibole shows a compositional range from predominantly actinolite to edenitic hornblende (Figure 10). Actinolite is anhedral in foliated glaucophane eclogites (Table 5; Figure 5a), occurs as inclusions in Grt1 (Figure 5a), or is found, together with

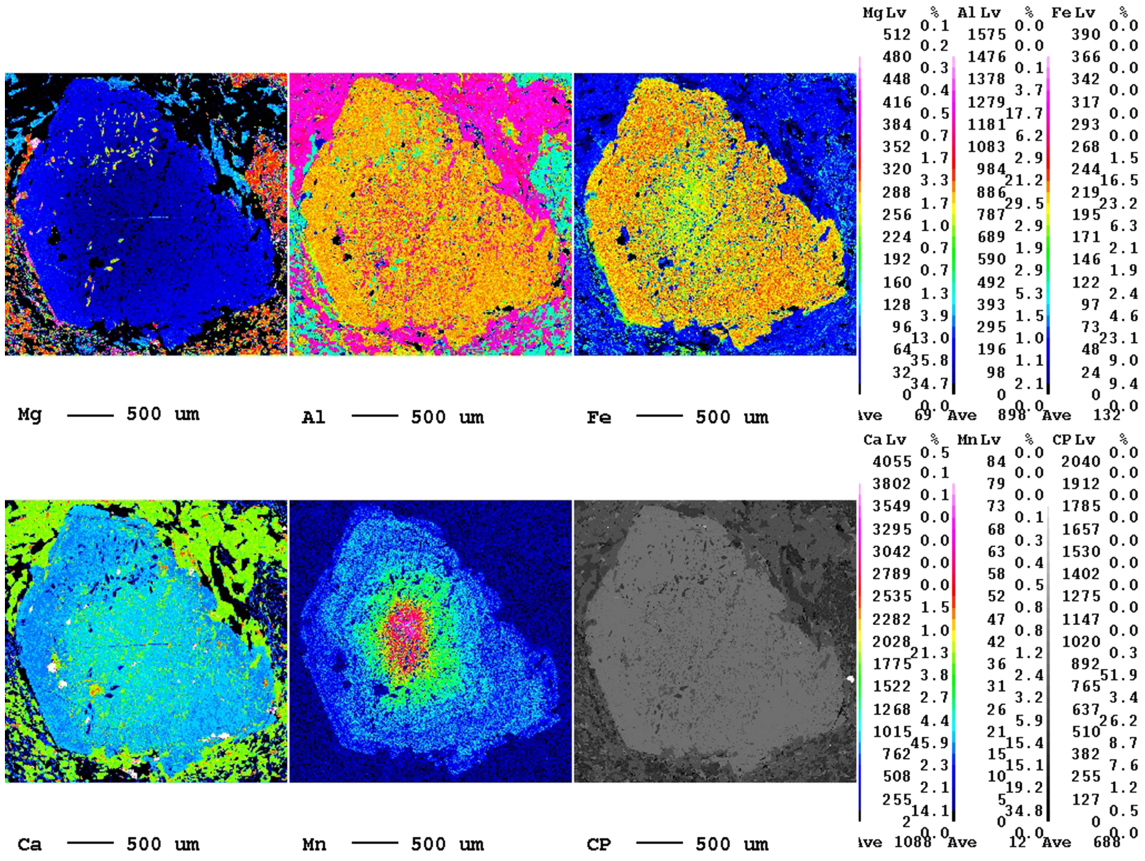

FIGURE 7 Major element distribution maps of Grt1 blast from sample SW108. Note the enrichment of Mn in the core and an oscillatory pattern for Mn towards the rim [Colour figure can be viewed at wileyonlinelibrary.com]

albite, as fine-grained symplectite replacing glaucophane (Table 5; Figures 8b and 9a) and omphacite (Table 5; Figures 5f and 8a). Locally, large poikiloblastic actinolite grains replace former glaucophane (Table 5; Figure 4f). More hornblende-rich compositions are only found in corona textures surrounding actinolite in foliated glaucophane eclogite (Table 5; Figure 9f) and in eclogite veins (Table 5; Figure 5c).

5.2.3 | Other phases

Chlorite is present as fibrous, sheaf-like aggregates in the blueschist matrix, it replaces garnet along the grain boundaries and fills up fractures in garnet (Table 5; Figure 9d). Similar to phengite, chlorite is more abundant within the blueschist than in the foliated glaucophane eclogite. Chlorite along fractures in garnet is inferred to be retrograde. However, in the matrix it may be part of the peak assemblage. Throughout the blueschist, chlorite does not show any significant compositional variations as X_{Mg} ranges from 0.42 to 0.48. Clinozoisite in blueschist is slightly richer in Al^{3+} compared to clinozoisite in eclogite veins (Table 6; Figure 9a; $X_{Fe} = 0.12–0.16$). Locally, clinopyroxene with a diopside-hedenbergite composition was found to be part of symplectites with albite (Table 3). Carbonate and apatite occur as interstitial, accessory crystals.

6 | BULK ROCK COMPOSITION OF THE ECLOGITE-VEINS, FOLIATED GLAUCOPHANE ECLOGITES AND BLUESCHISTS

The compositions of the Arbolle metabasites are listed in Table 7. In the case of the studied eclogite and blueschist samples, the silica content varies significantly from 44 to 51 wt%, Al_2O_3 ranges from 15.1 to 19.4 wt%, the Mg number (#Mg) is in the range 50–54 and the rocks can therefore be classified as derived from a primitive basaltic liquid. A higher content of CaO (up to 5–6 wt% CaO more than in omphacite-free blueschist) and a very low concentration of K_2O are found in samples in which the eclogite veins occur (Table 7). The low concentration of K_2O correlates further with the absence of phengite. By contrast, blueschists display lower CaO (~9 wt%) but higher K_2O and Na_2O than eclogites (Figure 11a).

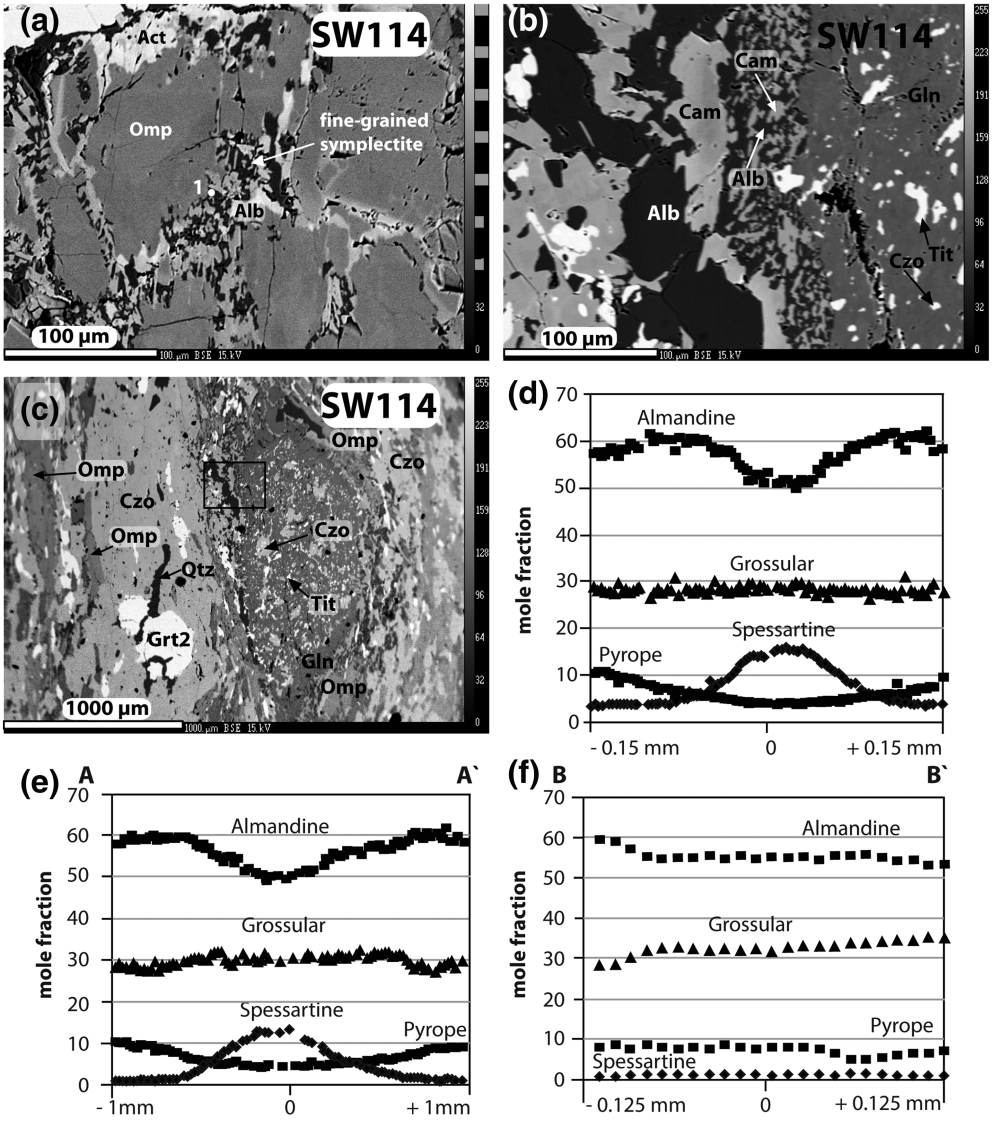

FIGURE 8 Backscattered electron images of selected microstructural domains of the eclogite-veins and adjacent foliated glaucophane eclogites investigated by EMPA: (a) a detailed view of omphacite replaced by symplectite of albite and Ca-amphibole. (b) A detailed view of albite and Ca-amphibole symplectite. (c) Large amphibole blast associated with eclogite-vein replaced by symplectite of albite and Ca-amphibole. The box represents the position of Figure 8b. (d) Representative EPMA zoning profile for Grt1 from the blueschist sample SW134 with diameter of 3 mm. (e,f) Representative EPMA zoning profile for Grt1 and Grt2 grains from the eclogite-vein + foliated glaucophane eclogite sample SW113, with diameters of 2 and 0.25 mm (traces A–A` and B–B` shown in Figures 4a and 5c). The dot shows the exact spatial location of analysed spot: (1) Pl, texture 2, Table 6

Eclogites and blueschists show a wide compositional range of incompatible trace elements, including Ti (0.77–2.58 wt% as TiO_2), Zr (85–205 ppm), Nb (10–34 ppm), and Y (21–34 ppm), although such elements are often considered relatively stable during metamorphism (Dal Piaz et al., 1981; Li et al., 2015; Zack & John, 2007). The trace element ratios of the samples plot partly in the fields of mid-ocean ridge basalt (MORB) and oceanic-island basalt (OIB) (Figure 11b). The large compositional variation of samples taken from the same outcrop may result from metasomatism on a local scale or distinct protolith chemistries or both. In contrast to the eclogites and blueschists, metagabbros display no comparable chemical variations (Table 7). Analysed metagabbros are very low in Zr, Ti, and Nb, while they have a high Cr content (258–418 ppm). This may be due to the accumulation process, mainly involving minerals with low concentrations of incompatible elements.

7 | METAMORPHIC CONDITIONS

Previous studies have indicated that the mafic suites of Mt. Emilius have preserved different stages of their evolution, such as pre-Alpine layered garnet–clinopyroxene–feldspar–hornblende-bearing amphibolites/granulites, Alpine *HP* mineral assemblages and decompressional re-equilibration (Angiboust et al., 2017; Dal Piaz et al., 1983; Lardeaux & Spalla, 1991). According to Pennacchioni (1996), rocks containing glaucophane are devoid of pre-Alpine relics. In this study, we also did not find pre-Alpine minerals, but pseudomorphs of glaucophane after pre-Alpine amphibole are clearly recognizable in the form of large blasts, showing a dusty appearance due to the presence of fine-grained inclusions (Compagnoni, 1977; Figures 4e,f and 8c). Since the lack of significant fluid infiltration suppressed reactions prior to eclogitization (Scambelluri et al., 1998) and Alpine *HP*

TABLE 3 Representative clinopyroxene composition of the Arbolle metabasite

Sample no.	SW113					SW114				
Mineral	Omp	Omp	Omp	Omp	Omp	Omp	Omp	Omp	Omp	Di
Texture	1	2	3	3	2	1	1	3	3	4
SiO_2 (wt%)	55.76	55.6	55.48	54.93	55.07	54.71	55.63	55.88	55.49	54.02
TiO_2	0.05	0.04	0.03	0.05	0.05	0.03	0.03	0.03	0.04	0.04
Al_2O_3	9.41	9.13	9.55	9.46	9.20	9.93	9.51	9.78	8.58	3.85
FeO	5.49	6.14	5.47	5.37	6.51	7.04	6.01	5.34	6.06	6.69
MgO	8.47	8.40	8.74	8.75	8.05	7.63	8.56	8.91	9.13	11.79
CaO	14.69	14.53	14.43	14.58	14.50	13.93	13.83	14.47	15.70	20.85
Na_2O	6.52	6.40	6.73	6.59	6.75	6.41	6.74	6.15	5.63	2.38
K_2O	0.01	0.00	0.02	0.00	0.00	0.00	0.01	0.01	0.00	0.02
Total	100.39	100.29	100.47	99.74	100.13	99.77	100.36	100.62	100.64	99.97
Si^{4+} (apfu)	3.99	3.99	3.97	3.97	3.98	3.97	3.99	3.98	3.98	3.98
Ti^{4+}	0.00	0.00	0.00	0.00	0.00	0.00	0.00	0.00	0.00	0.00
Al^{3+}	0.79	0.77	0.81	0.81	0.78	0.85	0.80	0.82	0.73	0.33
Fe^{2+}	0.33	0.37	0.33	0.32	0.39	0.43	0.36	0.32	0.36	0.41
Mg^{2+}	0.91	0.90	0.93	0.94	0.87	0.83	0.92	0.95	0.98	1.30
Ca^{2+}	1.13	1.12	1.11	1.13	1.12	1.08	1.06	1.11	1.21	1.65
Na^{+}	0.91	0.89	0.94	0.92	0.95	0.90	0.94	0.85	0.78	0.34
K^{+}	0.00	0.00	0.00	0.00	0.00	0.00	0.00	0.00	0.00	0.00
SUM	8.06	8.06	8.09	8.09	8.10	8.06	8.08	8.03	8.04	8.02
Acmite[a]	6.02	6.09	8.80	9.08	9.69	6.03	7.66	3.27	4.62	2.25
Jadeite	38.52	38.26	36.96	35.91	36.03	39.40	39.20	40.21	34.73	14.87
Di-Hed	55.46	55.65	54.23	55.01	54.28	54.56	53.14	56.52	60.65	82.88

Note: Totals include traces of Cr and Mn.

[a]Fe^{3+} contents were estimated by the calculating procedure: $Fe^{3+}{}_{Ac} = Na_{tot} - [Al_{tot} - (2(4\text{-}Si_{tot}))]$ if $Na_{tot} > Al_{tot}$ and $Fe^{3+}{}_{Ac} = Na_{Ac}$. (1) foliated glaucophane eclogite omphacite; (2) omphacite inclusion in Grt 1 of foliated glaucophane eclogite; (3) omphacite within eclogite-veins; (4) diopside symplectite within eclogite-veins.

metamorphic re-crystallization has gone to completion in the studied samples, the prograde Alpine metamorphic path was only preserved in the form of Grt1 compositional zoning and mineral inclusions. Although all Grt1 grains belong to the Alpine metamorphic cycle, are idioblastic and appear rather unresorbed along the rims, a detailed reconstruction of the prograde *P–T* evolution is difficult, because the Grt1 compositional zoning is not very pronounced. For example, the pressure-sensitive grossular component of garnet changes only slightly from the core to the rim (Figure 8d,e). It still seems reasonable to suppose that the blueschists and foliated glaucophane eclogites share a similar prograde history, as both lithotypes contain abundant Grt1 crystals with comparable chemical zoning features and glaucophane inclusions.

An adequate evaluation of peak metamorphism is strongly dependent on the selection of equilibrium parageneses. In omphacite-free blueschist pods the mineral assemblage Grt1 + glaucophane + phengite + clinozoisite + paragonite ± chlorite ± quartz is considered to document peak metamorphic conditions. In eclogite, however, the assemblage garnet ± omphacite ± clinozoisite ± glaucophane ± quartz is attributed to peak metamorphism. In this regard, it is important to note that glaucophane is confined to foliated glaucophane eclogites, where smoothly curved grain boundaries between glaucophane and omphacite indicate that they are in textural equilibrium. The absence of glaucophane inside the eclogite veins is presumably caused by the local variations of bulk rock chemistry between eclogite veins and the foliated glaucophane eclogite domains. This chemical gradient appears to be driven by the vein-forming fluid flow during *HP* metamorphism that did not attain a complete chemical equilibrium with the adjacent blueschist, on the scale of a hand specimen (Angiboust et al., 2017). The close

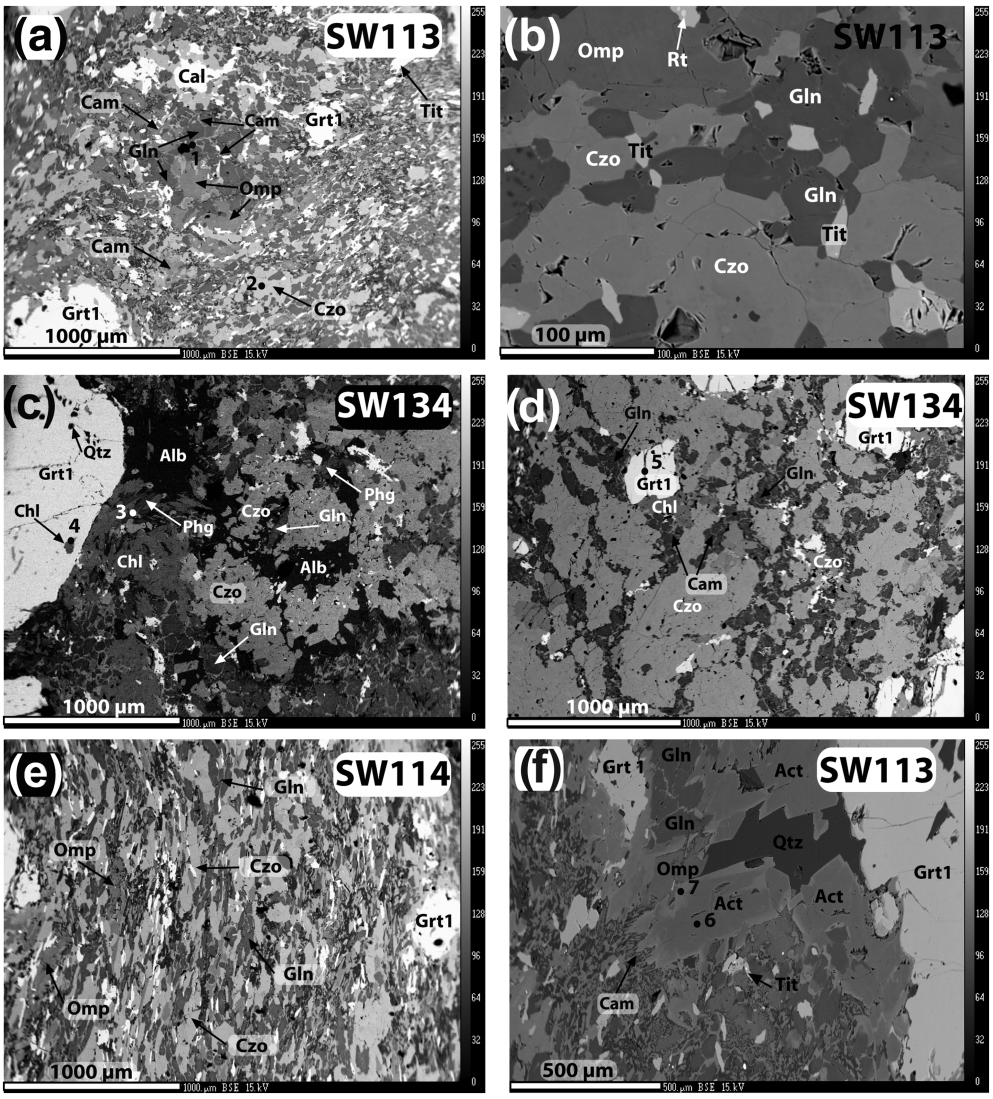

FIGURE 9 Backscattered electron images of selected microstructural domains of eclogite and omphacite-free blueschist investigated by EMPA: (a) mostly medium to fine-grained, high-strain volume of the foliated glaucophane eclogites. (b) Equilibrium texture between omphacite, glaucophane, clinozoisite and titanite in the foliated glaucophane eclogites. Note titanite contains small rutile inclusions. (c,d) Omphacite-free, low strain blueschists where the eclogite facies mineral assemblage of Omp + Grt2 is not developed. (e) Mostly medium to fine-grained, high-strain volumes of the foliated glaucophane eclogites. (f) Calcic amphibole in textural equilibrium with omphacite, glaucophane, clinozoisite and quartz, which is surrounded by amphibole of hornblende-rich composition. The dots show the exact spatial location of analysed spots: (1) Act, texture 4, Table 5, (2) Czo, texture 6, Table 6, (3) Phg, texture 1, Table 4, (4) Chl, texture 3, Table 4, (5) Chl, texture 4, Table 4, (6) Act, texture 8, Table 5, (7) Hbl, texture 6, Table 5

spatial association of eclogite veins and foliated glaucophane eclogites, however, indicates that the veins have also developed inside the glaucophane stability field. Another difficulty involves the stability of actinolite during eclogite-facies metamorphism. Actinolite has occasionally been found in textural equilibrium with omphacite, glaucophane, clinozoisite and quartz in the strain shadow of Grt1, indicating that it relates to the advanced prograde subducting path. This would imply that actinolite was present inside the foliated glaucophane eclogites prior to the pervasive deformation event, which led to the development of the *HP* foliation. However, as actinolite is clearly retrograde throughout the remainder of the high-strain matrix of the foliated glaucophane eclogites, it is not considered as part of the peak assemblage.

Using conventional thermobarometry on a variety of mineral pairs in eclogite led to *P–T* estimates which range from 400 to 560°C at 2.0 ± 0.3 GPa (Ellis & Green, 1979; Powell, 1985; Krogh, 1988; Table 8). Cpx-Grt temperatures of 490°C–553°C can be computed from omphacite inclusions in Grt1 porphyroblasts inside the foliated glaucophane eclogites for pressures of 1.7–2.3 GPa. Grt2 porphyroblasts in contact to vein omphacite give similar temperatures of 464°C–625°C for the same pressure range. Since all *P–T* results derived from texturally different mineral pairs are comparable, it can be assumed that eclogite-facies metamorphism occurred in a relatively narrow *P–T* range. Invariant *P–T* estimates from geothermobarometry are, however, strongly dependent on the equilibria among garnet, omphacite and an additional phase such as phengite

TABLE 4 Representative white mica and chlorite composition of the Arbolle metabasite

Sample no.	SW134				SW113		SW134	
Mineral	Phg	Phg	Pg	Pg	Chl	Chl	Chl	Chl
Texture	1	1	1	1	2	2	3	4
SiO_2 (wt%)	50.25	51.00	47.37	47.77	27.00	26.79	26.37	27.09
TiO_2	0.00	0.00	0.04	0.02	0.03	0.07	0.06	0.08
Al_2O_3	27.83	28.39	41.24	40.64	20.58	20.47	20.26	20.1
FeO	1.84	1.85	0.64	0.54	21.49	22.19	21.07	23.25
MnO	0.00	0.04	0.00	0.00	0.20	0.12	0.14	0.05
MgO	3.32	3.22	0.13	0.06	18.76	18.06	18.13	17.40
CaO	0.02	0.01	0.12	0.14	0.01	0.05	0.08	0.08
Na_2O	0.48	0.46	7.76	7.28	0.01	0.00	0.01	0.00
K_2O	10.81	10.28	0.50	0.42	0.00	0.01	0.00	0.03
Total	94.55	95.26	97.8	96.87	88.08	87.78	86.11	88.09
Si^{4+} (apfu)	3.37	3.41	2.95	3.01	2.77	2.77	2.77	2.80
Ti^{4+}	0.00	0.00	0.00	0.00	0.00	0.01	0.01	0.01
Al^{3+}	2.20	2.23	3.02	3.02	2.49	2.49	2.50	2.45
Fe^{2+}	0.10	0.10	0.03	0.03	1.84	1.92	1.85	2.01
Mn^{2+}	0.00	0.00	0.00	0.00	0.02	0.01	0.01	0.00
Mg^{2+}	0.33	0.32	0.01	0.01	2.87	2.78	2.83	2.68
Ca^{2+}	0.00	0.00	0.01	0.01	0.00	0.01	0.01	0.01
Na^{+}	0.06	0.06	0.94	0.89	0.00	0.00	0.00	0.00
K^{+}	0.93	0.88	0.04	0.03	0.00	0.00	0.00	0.00
SUM	7.00	7.00	7.00	7.00	9.99	9.98	9.98	9.97
XMg					0.46	0.45	0.46	0.42

Note: Totals include traces of Cr. $X_{Mg} = Mg/(Mg + Fe^{2+})$, (1) matrix phengite and paragonite in blueschist; (2) matrix chlorite in foliated glaucophane eclogite and blueschist; (3) chlorite in Grt1 in foliated glaucophane eclogite; (4) chlorite filling up cracks inside Grt1 in foliated glaucophane eclogite.

(Krogh Ravna & Terry, 2004). As phengite is absent in all studied eclogite assemblages, a garnet-omphacite-phengite equilibrium required for an accurate pressure estimate could not be defined. *P–T* calculations (Krogh Ravna & Terry, 2004) using Grt-Omp mineral pairs with phengite compositions from the adjacent blueschist are somewhat scattered and in parts lead to unrealistic low temperatures.

In order to corroborate *P–T* estimates from conventional thermobarometry, *P–T* pseudosections for the eclogite veins + foliated glaucophane eclogites and blueschist were computed in the NCFMASHO and NKCFMASHO model systems, respectively, using the Theriak-Domino software for bulk rock compositions from SW108, SW113, SW114, SW133, SW134, and SW135 (de Capitani & Petrakakis, 2010; Table 7; Figures 12 and 13). Phosphorus was not considered, because P_2O_5 is only present in accessory apatite. A similar consideration applies for TiO_2, because titanite is the dominant Ti-bearing phase and all other essential silicates do not contain appreciable TiO_2. Therefore, a CaO correction was conducted to adjust the input compositions. The K_2O content is generally very low in the eclogites (Table 7), and therefore has been omitted to simplify the diagrams. Because spessartine is concentrated in low amounts in garnet cores, MnO was neglected in all calculations. Since a reliable estimate for the amount of CO_2 present during *HP* metamorphism is difficult to make, the fluid phase is assumed to be pure H_2O. The Theriak-Domino calculations utilized thermodynamic data from Holland and Powell (1998). The following solid-solution models have been used: garnet (White et al., 2007), clinopyroxene (Green et al., 2007), amphibole (Diener et al., 2007), white mica (Coggon & Holland, 2002), and for chlorite and epidote (Holland & Powell, 1998). The application of solution models that account for Fe^{3+} incorporation in clinopyroxene and amphibole prevent epidote from being present everywhere in the pseudosections. Instead, with

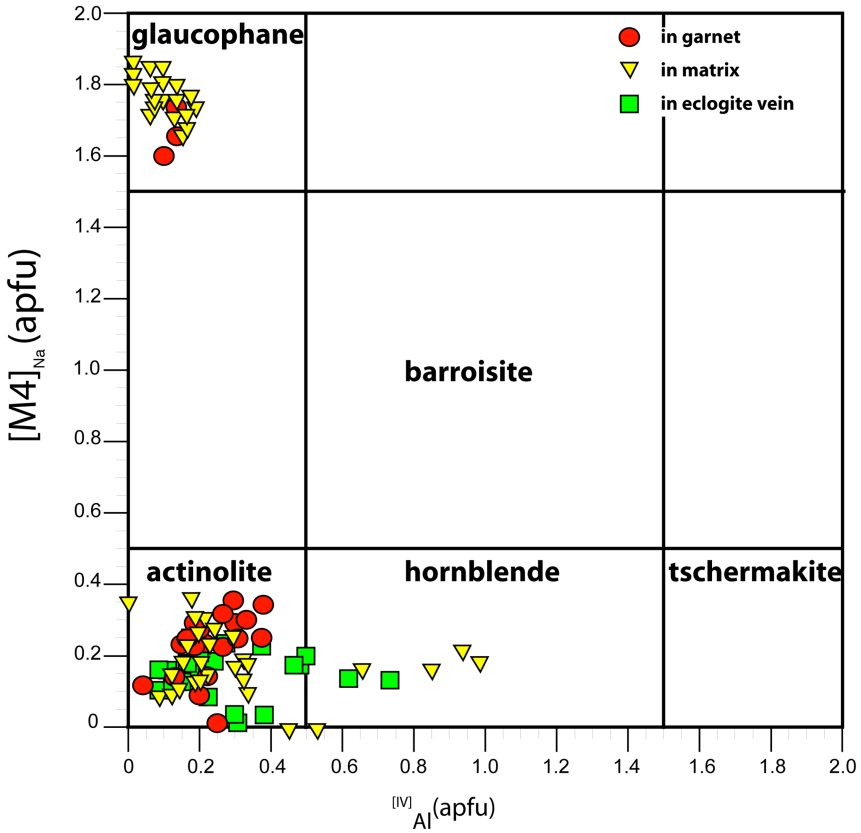

FIGURE 10 Compositional variations of amphibole from the Arbolle metabasites listed in Table 5. Amphibole nomenclature is after Locock (2014) [Colour figure can be viewed at wileyonlinelibrary.com]

increasing metamorphic grade, it can be expected that epidote would react out in the presence of amphibole or clinopyroxene. This is an important issue as clinozoisite is part of the diagnostic peak assemblage. Previous studies have pointed out the significant effect of $X_{Fe^{3+}}$ on pseudosection modelling and the resulting *P–T* constraints (Groppo & Castelli, 2010; Rebay et al., 2010). Since the ferric iron content has not been directly measured from the sample, the oxidation state is virtually unknown and can only be roughly estimated. In order to account for the uncertainties associated with the Fe^{3+}/Fe^{tot} ratio in the bulk-rock composition, several *P–T* pseudosections and garnet isopleths were calculated for each individual sample using various $X_{Fe^{3+}}$ values ranging from 10 to 20%. The choice of the trivalent iron content appears somewhat arbitrary. However, similar $X_{Fe^{3+}}$ values have been reported for other *HP* mafic rocks from the Western Alpine domain (Bocchio et al., 2000; Groppo & Castelli, 2010). To address how the disequilibrium between the eclogite veins and the foliated glaucophane eclogites affects the *P–T* estimations in this study, it is crucial to assess its impact on the effective bulk-rock composition during *HP* metamorphism. It is important to note in this regard that all calculated pseudosections for eclogites, showing distinct volume fractions of eclogite veins and foliated glaucophane eclogites, display a similar topology of phase relationships (see Supporting Information). Therefore, we believe that our *P–T* estimates for the eclogite samples presented in the following are robust and accurate, further supported by the considerable overlap in peak *P–T* estimates with the majority of other *P–T* data for the Western Alpine area (Angiboust et al., 2017). The eclogite sample SW113 and the blueschist sample SW134 were selected for a detailed discussion.

7.1 | *P–T* pseudosections of eclogite

To constrain peak metamorphic conditions, *P–T* pseudosections were calculated for the eclogite veins and adjacent foliated glaucophane eclogites in the NCFMASHO model system at $X_{Fe^{3+}} = 0.1$ (Figure 12a). In addition, the phase diagrams were contoured with compositional isopleths for garnet. The pseudosections predict the observed peak assemblage of the eclogite assemblage garnet + omphacite + clinozoisite + glaucophane + quartz in a narrow field of 550°C–600°C and 1.7–2.0 GPa. This field defines the metamorphic conditions where the eclogitization have proceeded, where the notable absence of kyanite in the eclogite samples leads to the maximum temperature limit of ~600°C. Calculated garnet isopleths, however, do not intersect within this stability field. Instead, the intersection of garnet isopleths

TABLE 5 Representative amphibole composition of the Arbolle metabasite

Sample no.	SW113									SW114		SW134
Mineral	Gln	Gln	Act	Act	Act	Hbl	Hbl	Hbl	Act	Gln	Act	Gln
Texture	1	2	3	4	5	6	6	7	8	9	10	11
SiO_2 (wt%)	57.90	58.42	56.04	55.41	55.81	48.67	49.34	48.91	54.96	57.63	54.91	58.36
TiO_2	0.01	0.04	0.02	0.03	0.02	0.10	0.00	0.09	0.06	0.03	0.04	0.04
Al_2O_3	11.28	11.7	3.26	2.73	3.03	8.78	8.70	6.18	2.74	10.29	3.51	11.57
FeO	9.12	8.69	9.27	9.34	8.19	13.43	15.78	15.71	9.70	10.33	9.50	6.90
MnO	0.00	0.02	0.10	0.07	0.02	0.01	0.02	0.18	0.01	0.04	0.00	0.00
MgO	11.00	11.47	17.39	17.65	17.44	13.98	11.35	12.46	16.94	11.33	17.47	12.42
CaO	1.38	0.77	10.7	11.49	11.30	10.82	9.66	11.07	12.20	2.13	11.12	0.88
Na_2O	7.19	7.52	1.92	1.31	1.49	2.97	3.02	2.08	1.22	6.36	1.55	6.85
K_2O	0.03	0.02	0.11	0.05	0.08	0.01	0.01	0.07	0.01	0.03	0.10	0.02
Total	97.94	98.74	98.84	98.11	97.96	98.85	97.89	96.88	97.84	98.20	98.27	97.05
Si^{4+} (apfu)	7.91	7.87	7.79	7.78	7.85	6.99	7.18	7.24	7.78	7.89	7.69	7.94
Al (VI)	0.09	0.13	0.21	0.22	0.15	1.01	0.82	0.76	0.22	0.11	0.31	0.06
Ti^{4+} (M1–M3)	0.00	0.00	0.00	0.00	0.00	0.01	0.00	0.01	0.01	0.00	0.00	0.00
Al (IV)	1.72	1.73	0.33	0.23	0.35	0.47	0.67	0.32	0.24	1.55	0.27	1.79
Mg^{2+}	2.24	2.31	3.61	3.69	3.66	2.99	2.46	2.75	3.57	2.31	3.65	2.42
Fe^{3+}	0.03	0.12	0.09	0.11	0.00	0.17	0.18	0.19	0.00	0.15	0.16	0.00
Fe^{2+}	1.00	0.83	0.97	0.97	0.96	1.35	1.69	1.73	1.15	0.99	0.91	0.78
Mn^{2+} (M4)	0.00	0.00	0.01	0.01	0.00	0.00	0.00	0.02	0.00	0.01	0.00	0.00
Fe^{2+}	0.01	0.03	0.02	0.02	0.00	0.09	0.05	0.03	0.00	0.04	0.04	0.00
Ca^{2+}	0.20	0.11	1.59	1.73	1.70	1.66	1.51	1.76	1.85	0.31	1.67	0.13
Na^{+}	1.79	1.86	0.38	0.24	0.30	0.24	0.44	0.19	0.15	1.64	0.29	1.77
Na^{+} (A)	0.12	0.11	0.14	0.11	0.11	0.59	0.41	0.41	0.19	0.05	0.14	0.03
K^{+}	0.01	0.00	0.02	0.01	0.01	0.00	0.00	0.01	0.00	0.01	0.02	0.00
A	0.12	0.11	0.16	0.12	0.12	0.59	0.41	0.42	0.19	0.05	0.15	0.04

Note: Totals include traces of Cr. Amphibole nomenclature is after Locock (2014). (1) matrix glaucophane; (2) glaucophane inclusion in large amphibole poikiloblasts; (3) large amphibole poikiloblasts; (4) actinolite rimming glaucophane; (5) actinolite inclusion in Grt1; (6) hornblende replacing glaucophane and actinolite; (7) hornblende intergrowth inside eclogite-vein; (8) actinolite in symplectites around omphacite; (9) glaucophane inclusion in Grt1; (10) matrix actinolite associated to clinozoisite; (11) glaucophane inclusion in Grt1.

indicates higher peak metamorphic conditions of about 2.2 ± 0.1 GPa at $550°C \pm 50°C$, which is in good agreement with previous estimates of Angiboust et al. (2017). These metamorphic constraints imply that, besides actinolite, lawsonite was part of the peak assemblage, even though neither lawsonite nor lawsonite pseudomorphs have been detected within the eclogitized domains studied here. This characteristic is commonly encountered in ophiolite suites of the Piemonte-Liguria ocean, since lawsonite seldom survives exhumation (Groppo & Castelli, 2010). Therefore, it may be reasonable to suppose that the eclogite veins have formed at the *P–T* conditions of the lawsonite-eclogite-facies, implying that lawsonite decomposed during subsequent retrogression (Hertgen et al., 2017).

Concerning the effects of choice of trivalent iron on the peak metamorphic conditions of eclogite, an interesting feature arises from Figure 12b, which was calculated for the same sample SW113 using $X_{Fe^{3+}} = 0.2$. Higher ferric iron contents significantly enlarge the stability field of talc towards lower metamorphic grades. This shows that with gradually increasing oxygen, more ferrous iron is converted to ferric iron, which in turn changes the bulk $Fe^{2+}/Fe^{2+} + Mg^{2+}$ ratio of the system (Rebay et al., 2010). This is supported by the observation that the overall stabilities of iron-free phases, such as lawsonite and kyanite, are not significantly affected by changing $X_{Fe^{3+}}$. In addition, while the first appearance of garnet does not change significantly due to higher ferric iron contents, the compositional garnet isopleths, which

TABLE 6 Representative plagioclase and clinozoisite composition of the Arbolle metabasite

Sample no.	SW114			SW113	SW114		SW113	
Mineral	**Alb**	**Alb**	**Alb**	**Alb**	**Czo**	**Czo**	**Czo**	**Czo**
Texture	**1**	**1**	**2**	**3**	**4**	**4**	**5**	**6**
SiO_2 (wt%)	68.14	68.28	68.05	67.62	36.71	37.44	38.00	38.32
Al_2O_3	20.69	20.98	20.17	20.11	27.71	27.83	26.97	28.19
FeO	0.13	0.17	0.02	0.35	7.50	7.72	8.63	7.18
MnO	0.00	0.00	0.00	0.03	0.04	0.04	0.13	0.16
MgO	0.00	0.00	0.00	0.08	0.04	0.07	0.01	0.02
CaO	0.91	1.08	0.58	0.23	24.02	24.15	24.32	24.4
Na_2O	10.31	10.89	11.99	12.05	0.03	0.01	0.03	0.01
K_2O	0.13	0.15	0.00	0.00	0.01	0.00	0.00	0.00
Total	100.32	101.56	101.08	100.52	96.19	97.44	98.21	98.35
Si^{4+} (apfu)	2.96	2.94	2.96	2.95	2.91	2.93	2.95	2.96
Al^{3+}	1.10	1.07	1.03	1.04	2.59	2.56	2.47	2.57
Fe^{3+}[a]					0.50	0.50	0.56	0.46
Fe^{2+}	0.01	0.01	0.01	0.01				
Mn^{2+}	0.00	0.00	0.00	0.00	0.00	0.00	0.01	0.01
Mg^{2+}	0.00	0.00	0.00	0.01	0.00	0.01	0.00	0.00
Ca^{2+}	0.04	0.10	0.03	0.01	2.04	2.02	2.03	2.02
Na^{+}	0.87	0.91	1.01	1.02	0.01	0.00	0.01	0.00
K^{+}	0.01	0.01	0.00	0.00	0.00	0.00	0.00	0.00
SUM	4.95	4.98	5.03	5.04	8.05	8.03	8.03	8.02
Albite	94.59	93.99	97.40	98.96				
Anorthite	4.62	5.17	2.60	1.04				
K-feldspar	0.78	0.83	0.00	0.00				
XFe					0.16	0.16	0.19	0.15

Note: Totals include traces of Cr and Ti.

[a]$X_{Fe} = Fe^{3+}/(Al^{3+} + Fe^{3+})$, recalculated assuming $Fe_{tot} = Fe^{3+}$, $X_{Fe} = Fe^{3+}/Fe^{3+} + Al^{3+}$, (1) late-stage albite vein in eclogite vein; (2) symplectite plagioclase in direct contact to omphacite; (3) matrix albite in foliated glaucophane eclogite; (4) vein forming clinozoisite; (5) clinozoisite inclusion in Grt1 in foliated glaucophane eclogite; (6) matrix clinozoisite in foliated glaucophane eclogite.

correspond to the measured compositions of Grt2, are shifted to lower pressure with increasing ferric iron content (Figure 12b). At this iron oxidation state, the isopleths define a consistent *P–T* window between 2.1 ± 0.1 GPa and 550 ± 50°C fitting the assemblage field of garnet + omphacite + lawsonite + glaucophane + quartz. This constraint, however, cannot be considered accurate because modelled and observed assemblages indicate lower peak metamorphic conditions. Besides garnet + omphacite + glaucophane + quartz, the observed mineral assemblage includes clinozoisite instead of lawsonite, which corresponds to a pressure maximum of about 2.0 GPa. Therefore, these conditions should be considered as a minimum peak metamorphic pressure. Given the combined uncertainties regarding lawsonite stability at peak conditions, the effective bulk-rock composition and the oxidation state of iron in our modelling approach, we conclude that the studied eclogite samples underwent peak *P–T* of 1.9–2.3 GPa and 550 ± 50°C. This estimate is derived from the entire spectrum of eclogite bulk compositions and $X_{Fe^{3+}}$ values considered (see Supporting Information).

7.2 | *P–T* pseudosections of blueschist

The computed NKCFMASHO *P–T* pseudosection for the blueschist for $X_{Fe^{3+}} = 0.1$ is illustrated in Figure 13a. Compared with the phase diagrams for the eclogite assemblages, the stability field of glaucophane is significantly enlarged whereas that of omphacite is reduced. This results from differences in the bulk rock

TABLE 7 XRF composition of selected Arbolle metabasites samples

Sample no.	SW108a	SW111a	SW113a	SW114a	SW115a	SW133a	SW134a	SW135a	SW109b	SW112b
Location	**E**	**E**	**E**	**E**	**E**	**B**	**B**	**B**		
SiO_2 (wt%)	44.76	45.75	46.01	45.44	45.62	48.51	49.29	49.66	51.74	50.45
TiO_2	2.01	2.41	2.40	2.57	2.58	1.35	1.35	1.36	0.38	0.28
Al_2O_3	17.73	15.53	15.47	15.08	15.03	19.05	19.37	19.42	14.34	16.35
Fe_2O_3 (T)[a]	11.20	11.25	11.22	11.49	11.46	10.51	10.58	10.64	3.61	4.30
MnO	0.19	0.17	0.19	0.16	0.17	0.16	0.17	0.16	0.09	0.09
MgO	5.11	5.86	5.73	6.24	6.16	5.62	5.68	5.77	9.29	9.51
CaO	15.35	14.81	14.80	15.24	15.31	8.98	9.15	9.09	14.82	13.5
Na_2O	2.15	2.47	2.53	1.88	2.01	3.33	3.30	3.22	2.94	2.65
K_2O	0.06	0.05	0.02	0.04	0.03	0.37	0.40	0.38	0.09	0.06
P_2O_5	0.32	0.29	0.43	0.31	0.45	0.21	0.07	0.21	0.01	0.02
LOI	1.20	0.66	1.10	0.74	1.05	1.61	0.71	1.48	1.27	2.00
Total	99.03	99.14	98.96	99.19	98.97	98.20	99.36	99.90	97.41	97.29
#Mg	50.07	53.38	52.89	54.42	54.16	54.03	54.13	51.38	84.98	82.94
Ba (ppm)	17	b.d.l.	b.d.l.	b.d.l.	b.d.l.	161	160	553	b.d.l.	b.d.l.
Co	34	35	39	40	40	21	22	14	21	29
Cr	214	220	239	232	234	82	85	222	418	258
Cu	51	24	17	9	9	14	13	40	37	47
Nb	23	29	29	34	34	10	10	16	3	3
Ni	138	194	160	182	179	22	21	28	79	154
Sc	31	31	30	31	33	27	26	17	62	48
Sr	666	478	481	490	493	313	308	251	188	309
V	214	216	241	235	240	217	218	174	175	131
Y	29	29	31	33	33	27	27	34	10	8
Zn	89	97	98	107	103	121	118	132	13	21
Zr	157	171	188	197	205	104	85	208	22	17
Rb	b.d.l.	4	b.d.l.	2	b.d.l.	9	9	18	b.d.l.	b.d.l.

Note: Major element composition is given in wt%. Trace element concentration is given in ppm. The Mg number (#Mg) has been calculated by the calculation procedure #Mg = 100 * [MgO/40.32]/[MgO/40.32] + [(0.9 * Fe2O3/1.11)/71.85], b.d.l. = below detection limit, E = eclogite veins + foliated glaucophane eclogites, B = blueschist, a metabasalt, b metagabbro.

[a]Total iron given as Fe_2O_3.

composition of the blueschist compared to the eclogite veins. Particularly, the presence of a higher Na content and lower Ca content in the bulk-rock composition of blueschist shifts the omphacite in line towards higher pressures and temperatures. This leads to the stabilization of the observed assemblage of garnet + glaucophane + phengite + paragonite + clinozoisite + quartz at metamorphic conditions of 1.5–1.8 GPa and 550°C–600°C. Since the timing of chlorite growth is ambiguous in the blueschist, it may be potentially considered as part of the peak assemblage. Its stability field requires temperatures of <560°C within this considered *P–T* window. However, the maximum possible pressures for the peak assemblage remain rather unchanged. The calculated garnet isopleths fit the garnet + glaucophane + phengite + lawsonite + chlorite + quartz field between 500 and 550°C at 2.0 ± 0.1 GPa. Using a higher $X_{Fe^{3+}}$ value of 0.2 for the same bulk rock, leaves the general phase equilibria relatively unchanged. The calculated garnet isopleths intersect within the garnet + glaucophane + phengite + paragonite + lawsonite + chlorite + quartz field at 1.8 ± 0.1 GPa and 550°C–500°C (Figure 13b). Since the spatial arrangement of garnet isopleths indicate lawsonite stability, which is consistent with previous findings (Angiboust et al., 2017; Hertgen et al., 2017) and close to the stability field of the observed mineral assemblage of garnet + glaucophane + phengite + paragonite + clinozoisite + quartz, the *P–T* estimate of 550 ± 50°C

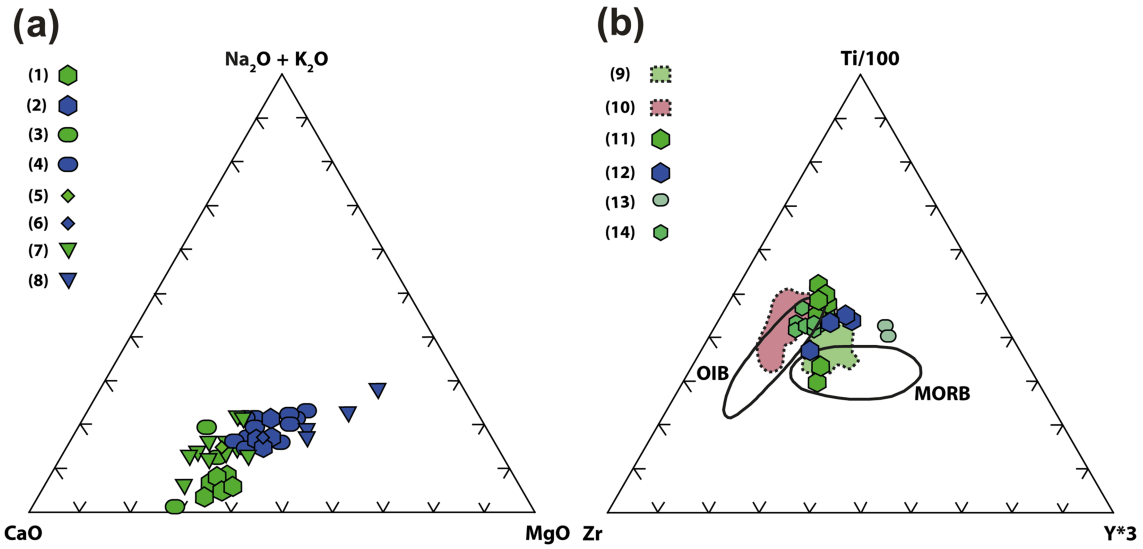

FIGURE 11 (a) Ternary diagram of the major elements CaO, MgO, and $Na_2O + K_2O$: (1) Eclogitc vein and foliated glaucophane eclogites from the Mt. Emilius (this study). (2) Blueschist from the Mt. Emilius (this study). (3) Eclogitic vein + selvages (Beinlich et al., 2010). (4) blueschist host and blueschist–eclogite transition zone (Beinlich et al., 2010). (5) Eclogite (Li et al., 2012). (6) Blueschist (Li et al., 2012). (7) Eclogite (van der Straaten et al., 2008). (8) Glaucophane-dominated blueschist (van der Straaten et al., 2008). (b) Incompatible trace element composition of metamafic rocks in the Ti-Y-Zr diagram of Pearce and Cann (1973): (9) the green highlighted area represents the compositional field of the ZSZ metabasalts from the Trockener Steg, the Lago di Cignana, and the Pfulwe and Täsch valley (Pfeifer et al., 1989; Weber & Bucher, 2015). (10) The red highlighted area represents the compositional field of the Etirol-Levaz slice and the Theodul Glacier Unit (Weber & Bucher, 2015). (11) and (12) Eclogite and blueschist samples from the Mt. Emilius (SW108, SW111, SW113, SW114, SW115, SW133, SW134, SW135). (13) Metagabbros from the Mt. Emilius (SW109, SW112). (14) ZSZ metabasalts from the Gressoney Valley and Valtournanche area (Dal Piaz et al., 1981). Ocean island basalts (OIB) and Mid-ocean ridge basalts (MORB) discrimination fields are illustrated after Li et al. (2015) [Colour figure can be viewed at wileyonlinelibrary.com]

TABLE 8 Compilation of P–T estimates obtained by geothermobarometry

Sample no.	SW113	SW114	SW115
Location	**E**	**E**	**E**
Krogh Ravna and Terry (2004)	Grt1 Omp (incl.) Phg 1.8–1.9 GPa 293°C–376°C	Grt2 Omp Phg 2.0–2.2 GPa 408°C–506°C	Grt2 Omp Phg 1.8–2.1 GPa 398°C–483°C
Krogh (1988)	Grt1 Omp (incl.) 1.7–2.3 GPa 490°C–503°C	Grt2 Omp 1.7–2.3 GPa 464°C–476°C	Grt2 Omp 1.7–2.3 GPa 565°C–579°C
Powell (1985)	Grt1 Omp (incl.) 1.7–2.3 GPa 517°C–529°C	Grt2 Omp 1.7–2.3 GPa 507°C–518°C	Grt2 Omp 1.7–2.3 GPa 589°C–602°C
Ellis and Green (1979)	Grt1 Omp (incl.) 1.7–2.3 GPa 541°C–553°C	Grt2 Omp 1.7–2.3 GPa 529°C–540°C	Grt2 Omp 1.7–2.3 GPa 612°C–625°C

Note: The derived temperatures are calculated with the Krogh (1988), Powell (1985), and Ellis and Green (1979) geothermometer for the pressure interval from 1.7 to 2.3 GPa. Note that derived pressure estimates using the Krogh Ravna and Terry (2004) calibration are based on Grt–Omp mineral pairs combined with phengite compositions from blueschist. For interpretation of the derived P–T estimates, see discussion in the text. Error bars of these methods are ± 65°C and 0.3 GPa (see Krogh Ravna & Terry, 2004). E = eclogite veins + foliated glaucophane eclogites, incl. = omphacite inclusions in Grt1.

and 1.8 ± 0.1 GPa is thought to represent the best estimate. In summary, it can be stated that eclogites and the adjacent omphacite-free blueschists experienced similar metamorphic conditions which overlap within the geological uncertainty. This correlation indicates that the major rock-forming mineral phases of both lithologies are stable under these *P–T* conditions, supporting the idea that they coexisted during peak metamorphism.

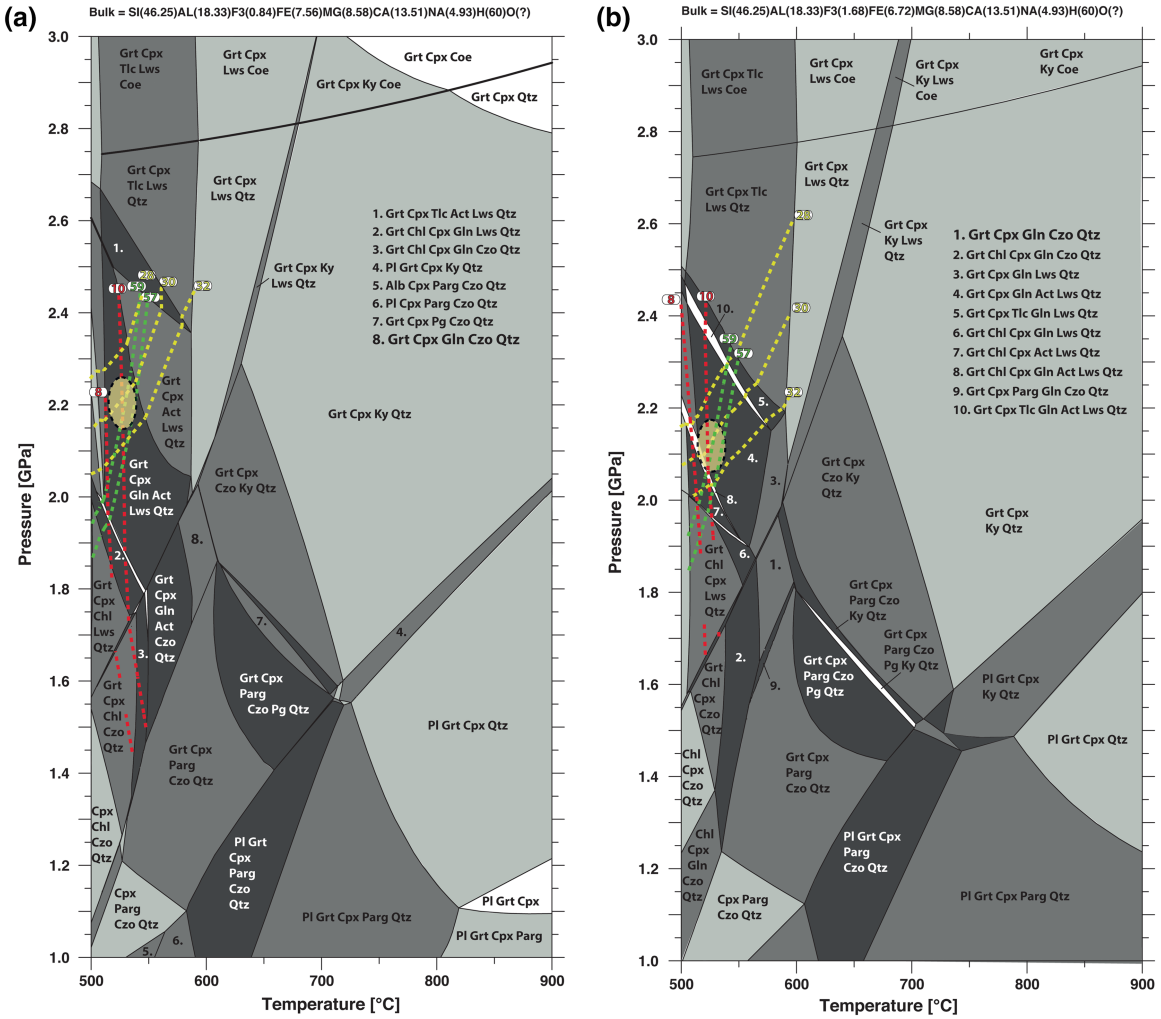

FIGURE 12 (a,b) *P–T* pseudosections for the representative eclogite-vein + adjacent foliated glaucophane eclogite assemblage of sample SW113 calculated with $X_{Fe^{3+}} = 0.1$ and 0.2 in (a) and (b), respectively. Bulk-rock compositions have been recalculated on atomic basis and the results are given at the top of each stability diagram. Both diagrams were calculated with water in excess. Only a selection of relevant assemblage fields is labelled. Univariant reactions are shown as continuous lines. Four phase fields are highlighted in light grey. Five phase fields are highlighted in dark grey. Six phase fields are dark shaded. Three and seven phase fields are unshaded. The pseudosection is contoured with isopleths of the almandine (green), pyrope (red) and grossular (yellow) contents in garnet, which correspond to measured compositions of Grt1 (Table 2). The yellow ellipses correspond to the intersection of compositional isopleths outside the stability field of the observed eclogite assemblage Grt–Omp–Gln–Czo–Qtz [Colour figure can be viewed at wileyonlinelibrary.com]

8 | Lu–Hf GEOCHRONOLOGY

The studied sample is a foliated glaucophane eclogite with eclogite veins. A separation of the two garnet generations was not possible. We made four analyses of whole-rock powder and seven of garnet separates (Table 9). Two of the whole-rock splits were completely digested ("bombed") and two were selectively digested ("tabletop") in order to minimize the effect of inherited inclusions, for example, zircon. Respectively all four whole-rock splits in combination with the seven garnet separates yielded identical age results within error, ranging from 52.3 ± 3.8 Ma with a MSWD of 5.3 to 53.9 ± 3.3 Ma with a MSWD of 5.0. This shows that inherited inclusions are insignificant. The relatively high errors and MSWDs result from one off-isochron garnet analysis (Figure 14). Leaving this analysis away, the remaining six garnet analyses yield very well-defined isochrons ranging from 52.96 ± 0.91 Ma with a MSWD of 1.3 to 54.43 ± 0.83 Ma with a MSWD of 1.7. To exclude any effects of inherited phases we chose the age of 52.96 ± 0.91 Ma obtained from a tabletop-digested whole-rock analyses and six garnet splits as the best approximation to the actual age of formation of eclogite. The one outlier analysis may have resulted from an analytical problem. It is also possible that this garnet separate contained more late stage garnet

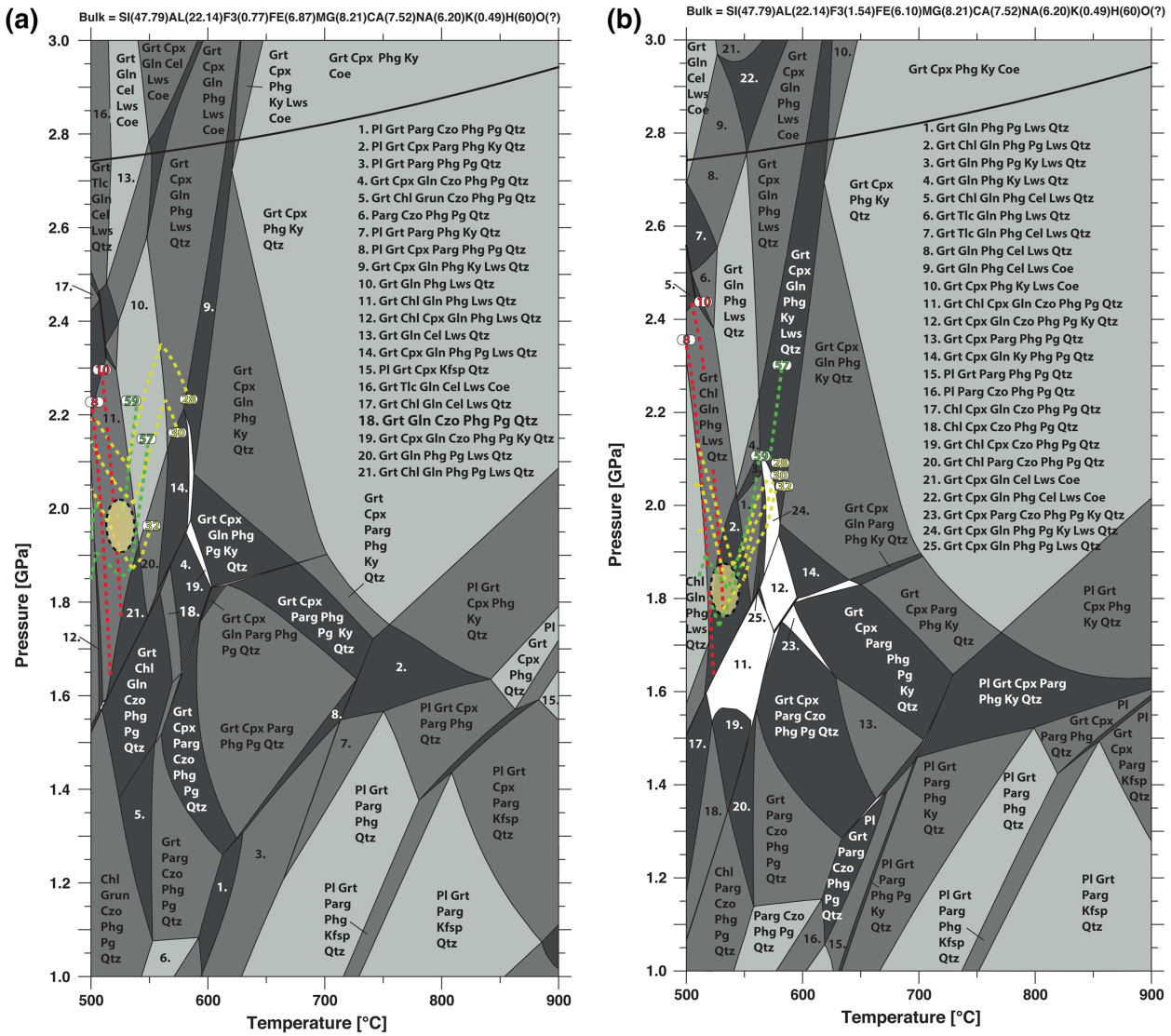

FIGURE 13 (a,b) *P–T* pseudosection for the representative blueschist of sample SW134 calculated with $X_{Fe^{3+}} = 0.1$ and 0.2 in (a) and (b), respectively. Bulk-rock compositions have been recalculated on atomic basis and the results are given at the top of each stability diagram. Both diagrams were calculated with water in excess. Only a selection of relevant assemblage fields is labelled. Univariant reactions are shown as continuous lines. Five phase fields are highlighted in light grey. Six phase fields are highlighted in dark grey. Seven phase fields are dark shaded. Eight phase fields are unshaded. The pseudosection is contoured with isopleths of the almandine (green), pyrope (red), and grossular (yellow) contents in garnet, which correspond to measured compositions of Grt1. The yellow ellipse indicates the intersection of compositional isopleths corresponding to the measured compositions of Grt1 metamorphism close to the field of stable Grt–Gln–Phg–Pg–Czo–Chl–Qtz [Colour figure can be viewed at wileyonlinelibrary.com]

(Grt2) than the other separates, which is indicated by the comparatively low Lu/Hf and Hf/Hf.

9 | DISCUSSION

9.1 | Coexistence of eclogite and blueschist rocks

The close spatial association of eclogite and blueschist in the field suggests a genetic link between these two rock types. Pseudosection calculations in this study support this assumption since within error the *P–T* conditions of the eclogitic veins, foliated glaucophane eclogites, and the blueschists are similar. Thermodynamic modelling results in estimates of 1.9–2.3 GPa at 550 ± 50°C for eclogite and 1.8 ± 0.1 GPa at 550 ± 50°C for the adjacent blueschist (Figures 12 and 13). The intermediate *P–T* space at about ~1.9 GPa marks the gradual transition zone where the diagnostic minerals of blueschists and eclogites may occur as a stable association (Gao et al., 2007; Gao & Klemd, 2001). Thus, the overlapping

TABLE 9 Lu–Hf isotope compositions of the whole rock and garnet separates

Type	Lu (ppm)	Hf (ppm)	$^{176}Lu/^{177}Hf$	± 2 SD	$^{176}Hf/^{177}Hf$	± 2 SD
WR1 (tt)	0.355	0.246	0.2052	0.0004	0.283052	0.000015
WR2 (tt)	0.332	0.248	0.1897	0.0004	0.283045	0.000031
WR1 (b)	0.374	3.34	0.01589	0.00003	0.282806	0.000015
WR2 (b)	0.363	2.94	0.01752	0.00004	0.282832	0.000018
Grt1	1.51	0.109	1,965	0.004	0.284842	0.000051
Grt2	1.59	0.123	1,835	0.004	0.284535	0.000045
Grt3	1.63	0.102	2,276	0.005	0.285093	0.000103
Grt4	1.69	0.098	2,442	0.005	0.285203	0.000071
Grt5	1.50	0.083	2,562	0.005	0.285384	0.000107
Grt6	1.78	0.118	2,142	0.004	0.284959	0.000085
Grt7	1.66	0.123	1,916	0.004	0.284747	0.000072

Note: tt, low-pressure (table top) digestions; b, high-pressure (bombed) digestions.

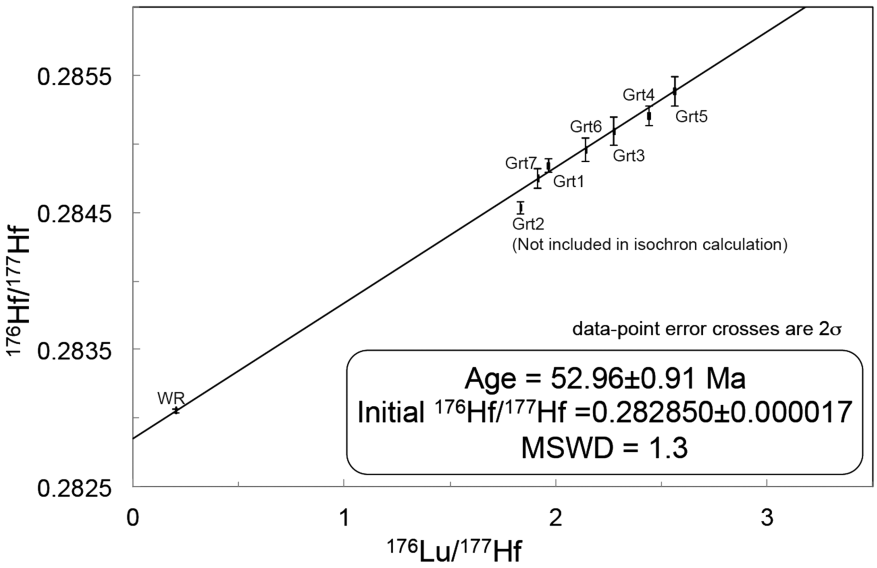

FIGURE 14 Lu–Hf garnet-whole rock isochron plot for sample SW108 from the Mt. Emilius klippe. See Table 9 for data used to calculate the isochron

field of the metamorphic peak constraints for the eclogites and blueschist defines the metamorphic conditions where the inferred assemblages can coexist (Figure 15). These inferences are in good agreement with the majority of *P–T* data for the ZSZ and associated *HP* continental slices, which are aligned along a cold geothermal gradient of 7–9°C/km. The interpretation that the blueschists in the Mt. Emilius sliver formed at or close to the metamorphic peak differs from many previous studies in the Piemonte meta-ophiolites, which linked blueschist-facies rocks to the prograde or retrograde path (Barnicoat & Fry, 1986; Bearth, 1967; Ernst, 1988; Meda et al., 2010; Pfeifer et al., 1989; Pognante, 1991). Bearth (1967), for instance, emphasized that many glaucophanites throughout the ZSZ preserved omphacite inclusions in garnet porphyroblasts, indicating that these rocks underwent eclogite-facies metamorphism prior to blueschist-facies retrograde overprint. Although the blueschists investigated in this study are similar to the glaucophanites in the ZSZ, the possible coexistence of eclogites and blueschists during *HP* metamorphism is supported by the following petrographical observations: (1) No relicts of Grt2 or Omp have been detected in blueschist. If the blueschists represented intensely retrogressed eclogites, it appears likely that at least some relics of former Grt2 or Omp would have been preserved. This corresponds well with the lack of glaucophane inside the eclogite veins. (2) Grt1 crystals within blueschist lack omphacite inclusions, while such inclusions are common in Grt1 porphyroblasts of foliated glaucophane eclogites. By contrast, glaucophane inclusions are common in both eclogite and blueschist. This is supported by blueschist Grt1

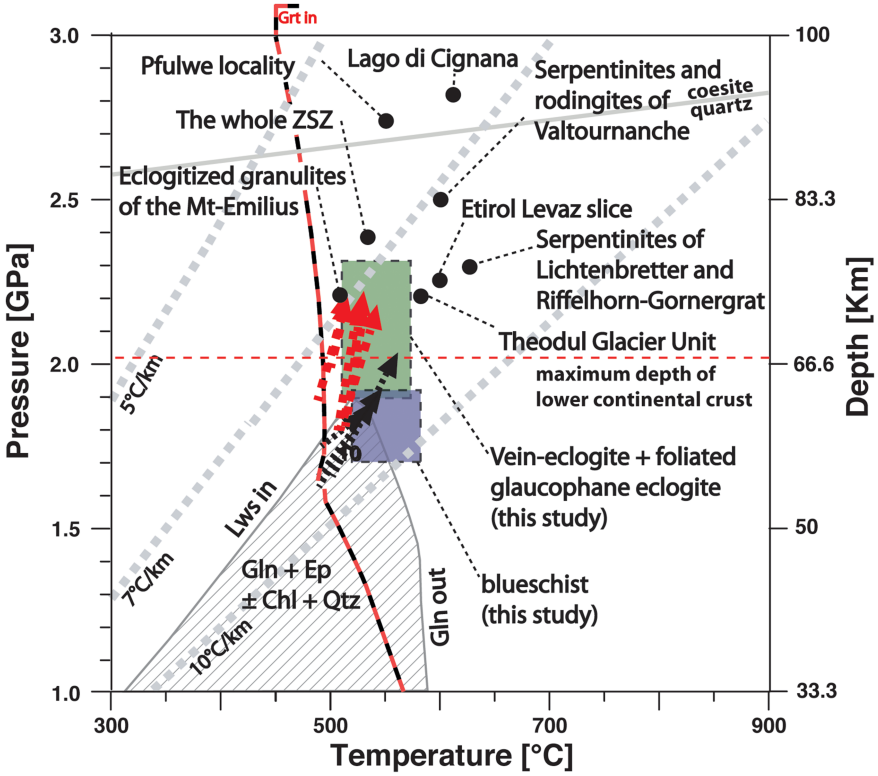

FIGURE 15 Compilation of maximum *P–T* data derived for the Penninic Alps: Lago di Cignana (Reinecke, 1991), Pfulwe locality (Bucher et al., 2005), the whole ZSZ (Angiboust et al., 2009), serpentinites of the Lichenbretter and Riffelhorn-Gornergrat (Li et al., 2004), serpentinites and rodingites of Valtournanche (Rebay et al., 2012; Zanoni et al., 2016), eclogitized granulites of the Mt Emilius (Angiboust et al., 2017), Etirol Levaz slice (Fassmer et al., 2016), Theodul glacier unit (Weber & Bucher, 2015). The prograde path of eclogite + adjacent blueschist assemblages deduced by garnet compositional isopleths is indicated by reddish arrows, while the thin black arrows illustrate the prograde path of the hosting blueschists. Dark green shaded area represents peak *P–T* estimate for the eclogite assemblages of this study, while the bluish field shows peak *P–T* estimate for the blueschists. Note the overlap field for both lithotypes at 1.9 ± 0.1 GPa and 550 ± 50°C. Dashed grey lines correspond to different geothermal gradients. The dashed black-red line represents the garnet-in boundary. The striped field represents the prograde assemblage of glaucophane + clinozoisite + chlorite + quartz in the absence of lawsonite computed by pseudosection modelling [Colour figure can be viewed at wileyonlinelibrary.com]

having a composition similar to eclogite Grt1 and most Grt1 grains appearing almost unresorbed along their rims. (3) Compared to the foliated glaucophane eclogites, the blueschists are more coarse-grained and display pervasive recrystallization to a much lower degree. This structural difference results from escaping the penetrative eclogitization rather than decompressional re-equilibration (Pennacchioni, 1996).

A shared prograde path may further support the contemporaneous existence of eclogites and blueschists near peak metamorphic conditions. However, as mentioned earlier, the prograde *P–T* path is hard to reconstruct by computed pseudosections because the related matrix assemblages are absent. In an attempt to deduce at least some parts of the prograde metamorphic evolution, the intersection of garnet isopleths corresponding to the observed zoning trends of Grt1 porphyroblasts of both eclogites and blueschists were used (Figure 15). The progressive increase in pyrope and almandine from core to rim combined with minor changes in grossular suggests a clockwise prograde *P–T* path, which commences at temperatures of 480°C–520°C and pressures of 1.6–1.9 GPa. The termination of the derived prograde *P–T* path is indicated by garnet rim compositions at 520°C–560°C and 1.8–2.2 GPa, which coincides with the inferred peak metamorphic conditions for both lithotypes. All *P–T* trajectories represent the later stages of prograde metamorphism and fit the typical geothermal gradient of fast subduction environments between 7 and 9°C/km. It should be noted, however, that the interpreted prograde paths for eclogite and blueschist samples are not identical in shape, but the blueschists lie on a higher geothermal gradient than the prograde conditions derived for the eclogite assemblages. Nevertheless, the prograde development of all studied samples occurred in the stability field of glaucophane + clinozoisite + quartz culminating at peak pressures of 1.9 ± 0.1 GPa, as deduced from mineral inclusions in garnet and garnet zoning. The consideration

that the eclogites and blueschists shared parts of the prograde path and equilibrated under similar peak metamorphic conditions is in accordance with previous studies from several *HP* terrains that have demonstrated that interlayered eclogites and blueschists reached the same or at least comparable peak conditions (Beinlich et al., 2010; Li et al., 2012; Vitale Brovarone et al., 2011). The stable coexistence of eclogite- and blueschist-facies mineral assemblages is thought to be the result of distinct whole-rock compositions (Beinlich et al., 2010; Li et al., 2012; Wei & Clarke, 2011). All these studies have ascribed the significant compositional variations of the *HP* rocks not to different protolith compositions but to variable degrees of metasomatism during fluid infiltration under *HP* conditions.

9.2 | Formation of eclogitic veins during shear zone development

At the studied site, eclogitic reaction selvedges are confined to places where eclogite veins occur. Ubiquitous dynamic microstructures of shape-preferred omphacite, including undulose extinction and subgrain boundaries, within both eclogite veins and foliated glaucophane eclogites indicate that eclogitization was accommodated by ductile deformation. These microstructures of omphacite have been reported as characteristic for fluid-deposited, syntectonic *HP* veins for eclogite-facies rocks in the Western Alps (Hertgen et al., 2017; Pennacchioni, 1996; Philippot & Selverstone, 1991; Widmer & Thompson, 2001). Within the foliated glaucophane eclogites, pervasive recrystallization led to the formation of a foliated eclogite-facies mineral assemblage and strongly reduced the grain size, which shows these domains underwent high shear stresses that led to the nucleation of ductile shear zones and were linked to eclogite vein formation. Compared to the whole rock composition of the blueschists in close proximity, localized eclogitization along shear zones was also accompanied by a marked CaO enrichment, a decrease in K_2O, and decomposition of hydrous phases, which probably resulted from fluid–rock interaction processes during shear zone formation (Angiboust et al., 2017). Along the interface between eclogitic veins and blueschist wall rocks, the foliated glaucophane eclogite is interpreted to result from these fluid–rock interaction processes in form of in-situ dehydration of the precursor blueschist and the veins are thus classified as dehydration veins (Gao & Klemd, 2001). The compositional differences between eclogites and blueschists may, however, also be ascribed to distinct protolith chemistries before Alpine metamorphism. The interpretation that compositional heterogeneities are inherited from the protolith appears less likely since whole rock compositional variations in major elements are undoubtedly dependent on the eclogite-vein formation mechanism.

9.3 | Transformation of blueschist to eclogite by reactive fluid flow in subducted continental crust

As inferred from *P–T* pseudosections, the eclogite veins, foliated glaucophane eclogites, and the adjacent blueschists have undergone similar peak metamorphic conditions but developed different *HP* mineral assemblages, which in turn is linked with distinct bulk-rock chemistries. From the combined geological evidence and context presented above it follows that both eclogites and blueschists underwent a heterogeneous reaction history. This implies that a sequence of mineral reactions took place in domains where eclogitization proceeded, while this metamorphic transformation was absent inside the blueschist pods. In this context, it is significant that the eclogite veins and foliated glaucophane eclogites are almost completely devoid of phengite, paragonite, and chlorite, while these hydrous phases are abundant in the adjacent blueschist. This shows that the formation of eclogite veins occurred as a dehydration of the precursor blueschist accompanied by the loss of alkalis (indicated by the absence of phengite). In metabasites, it is widely accepted that the breakdown of glaucophane is the most important process of dehydration during eclogitization. According to this, the transformation of blueschist- to eclogite-facies parageneses at 500°C–600°C and 1.9 GPa has been described by several dehydration reactions (Gao & Klemd, 2001) such as

$$5\,\mathrm{Czo} + 13\,\mathrm{Gln} = 9\,\mathrm{Pyrope} + 26\,\mathrm{Jadeite} + 12\,\mathrm{Diopside} + 19\,\mathrm{Qtz} + 15\,\mathrm{H_2O}. \quad (1)$$

$$1\,\mathrm{Pg} + 1\,\mathrm{Gln} = 1\,\mathrm{Pyrope} + 3\,\mathrm{Jadeite} + 2\,\mathrm{Qtz} + 2\,\mathrm{H_2O}. \quad (2)$$

Reactions 1 and 2 account for many textural observations presented above. However, they do not explain the entire consumption of phengite inside the eclogite veins. The controlling reaction that describes the observed mass transfer of alkalis, for example, potassium, and forms the eclogite reaction products can be adequately described as

$$2\,\mathrm{Phg} + 3\,\mathrm{Gln} = 3\,\mathrm{Pyrope} + 6\,\mathrm{Jadeite} + 9\,\mathrm{Qtz} + 5\,\mathrm{H_2O}\,(\text{with dissolved } \mathrm{K_2O}). \quad (3)$$

This dehydration reaction leads to the crystallization of an eclogite-facies assemblage and transfers the

released potassium away from the eclogitized domain. There is, however, no direct textual evidence for the reaction, which is probably due to the completeness of the dehydration process. The reaction can only be indirectly derived from the significant differences in bulk rock composition between the closely neighbouring blueschist and eclogite assemblages.

Based on garnet textures presented above, it can be inferred that garnet growth can be linked to two growth stages. From the blueschist pods, across the foliated glaucophane eclogites towards the eclogite veins a change in mineral content can be found, where Grt1 + glaucophane are present in blueschist pods, Grt1 + omphacite + glaucophane occur in the foliated glaucophane eclogites, whereas the eclogite veins lacking glaucophane and comprise Grt2 + omphacite. This sequence of distinct garnet-bearing mineral assemblages indicates that Grt2 and omphacite grew at the expense of Grt1 and glaucophane during the development of eclogite veins. Based on this observation, the following reaction maybe defined

$$\text{Grossular} + 2\,\text{Gln} = 4\,\text{Jadeite} + 3\,\text{Diopside} + \text{Pyrope} + 2\,\text{Qtz} + 2\,\text{H}_2\text{O}. \quad (4)$$

This balanced reaction implies garnet progressively shifts towards pyrope-rich compositions. However, Grt2 and Grt1 are chemically similar. This correlates with the fact that they formed in a relatively narrow *P–T* range close to peak conditions. Therefore, mobile components in the above isochemical reaction 4 must be added to the immediate reaction site to decompose glaucophane. As demonstrated recently by Angiboust et al. (2017) and Hertgen et al. (2017), eclogitization within the Mt. Emilius sliver is intimately coupled to pervasive deformation and fluid infiltration causing an unusual Ca-rich bulk composition. This suggests that the reactions transforming blueschist to eclogite were not isochemical but the incoming fluid added Ca. The supply of fluids allowed for the necessary introduction of mobile components to form high modal abundances of omphacite without a substantial change in garnet composition.

The reactions discussed above are responsible for the spatially limited development of eclogite veins in the continental crust of the Mt. Emilius sliver, whereas the blueschists remained unaffected. Within lower crustal terrains, unreacted rocks adjacent to major fluid conduits are usually attributed to slow solid-state reaction kinetics under fluid absent conditions (Leech, 2001). The blueschists investigated in this study, however, cannot be regarded as "dry" rocks, since they contain high amounts of structurally bound water (~6 wt%). Therefore, the absence of the eclogite-forming reactions in blueschist is not the result of slow solid-state reaction kinetics but to the absence of the Ca-rich fluid. Metamorphic reactions leading to eclogitization are linked to locations where deformation along shear zones allows fluids to induce significant chemical modifications of the bulk rock. The cause of local Ca-metasomatism and the source of the water are not known with certainty, but we assume that the Monte Emilius slice was accreted to the orogenic wedge above the subduction zone and impregnated by Ca-rich fluid from downgoing oceanic crust underneath (Angiboust et al., 2017).

9.4 | Tectonic implications

The similar *P–T* conditions recorded by blueschist and eclogite vein assemblages, 1.8 ± 0.1 GPa/550 ± 50°C and 1.7–2.0 GPa/550–600°C, respectively, suggest that there was not a long time between the formation of these two rock types. The Monte Emilius sliver consisted of continental crust that experienced high-temperature/low-pressure metamorphism in the Permian, resulting in dry conditions. During Palaeocene to Early Eocene, it was subducted to 60 or 70 km depth. There, blueschist formed by hydration of a mafic rock. The rocks were then accreted to the hanging wall of the subduction zone and invaded by a different fluid, rich in Ca, probably derived from the downgoing oceanic crust underneath.

The sample which we dated using Lu–Hf includes both eclogite veins and foliated glaucophane eclogites and also includes garnets of both generations. If the two garnet generations were of significantly different age, the dating would not have yielded such a well-defined isochron. The well-defined isochron also shows that there is no significant effect of the oscillatory garnet growth on the obtained age. Therefore, the dating leads to the same result as the petrological study, that the formation of blueschist was closely followed by the formation of the eclogite veins, and the entire process occurred at about 53 Ma, in the Early Eocene (52.96 ± 0.91 Ma).

The age of *HP* metamorphism at Monte Emilius, ~53 Ma, is in accordance with previous Lu–Hf dating from other continental slivers in the same tectonic level, the Theodul Glacier Unit (Weber et al., 2015) and the Etirol-Levaz Unit (Fassmer et al., 2016) which gave ages of 62 to 52 Ma. Lu–Hf ages from the underlying Zermatt-Saas ophiolites, however, are systematically slightly younger, between ~52 and ~38 Ma (Skora et al., 2015). This is at odds with the hypothesis that the continental slivers represent extensional allochthons emplaced by rifting in the Zermatt-Saas oceanic basin (Beltrando et al., 2010) because in that case the slivers should have been subducted together with the ophiolites

and should yield the same ages as the ophiolites. Instead, the slivers may have been derived from the northwestern margin of the continental block that formed the Sesia-Dent Blanche Nappe (Lardeaux & Spalla, 1991; Pleuger et al., 2007; Roda et al., 2012). On the other hand, new zircon age constraints of serpentinites imply that some portions of the Zermatt-Saas ophiolites may have undergone *HP* metamorphism at 65.5 ± 5.6 Ma (Rebay et al., 2018), which are comparable to those already reported for the Sesia-Dent Blanche Nappe (Rubatto et al., 1999). In case of the Theodul Glacier Unit, three Lu–Hf garnet ages of 50–49 Ma coincide in time with the Alpine metamorphism in the surrounding metaophiolites (Bovay et al., 2021). These findings support the interpretation that the continental slivers were subducted contemporaneously with the oceanic crust of Zermatt-Saas. However, such type of tectonic model is not supported by the results of this study. In any case, initial subduction of the Zermatt-Saas ophiolites may have released the Ca-rich fluid responsible for metasomatism of our samples.

10 | CONCLUSIONS

Pseudosection modelling in this study revealed that eclogite and adjacent omphacite-free blueschist in the Mt. Emilius sliver are stable at 1.9–2.3 GPa/550 ± 50°C and 1.8 ± 0.1 GPa/550 ± 50°C and coexisted at pressures of about ~1.9 GPa and temperatures of 550 ± 50°C. The stability of distinct *HP* mineral assemblages in these lithotypes is due to differences in the respective bulk-rock composition (in particular the CaO content). Compositional variations in the eclogite-veins and blueschists are not ascribed to different protolith compositions but are interpreted to result from variable degrees of metasomatism, which result in different reaction histories during Alpine *HP* metamorphism. At sites where metasomatism occurs the blueschist is converted into an eclogite assemblage, whereas blueschist outside the veins was preserved during peak metamorphism.

The results presented herein also imply that blueschist-facies mineral assemblages in the internal Western Alps have developed at different stages. In many cases, these assemblages were interpreted to have formed during prograde metamorphism. Other Western Alps blueschists have been related to decompression during exhumation. In the present study, however, both lithologies have formed under comparable *P–T* conditions close to peak metamorphism, where a Ca-rich bulk rock favoured eclogite-facies mineral assemblages whereas lower CaO contents stabilized blueschist-facies assemblages.

Our Lu–Hf dating suggests that the subduction of Monte Emilius to 60–70 km depth and the Ca metasomatism by externally-derived fluids occurred almost at the same time, at ~53 Ma in the Early Eocene. We assume that the fluids were released by the Zermatt-Saas oceanic crust which was starting to descend in the subduction zone underneath.

ACKNOWLEDGEMENTS

The authors are thanked for valuable assistance of T. Nagel and D. Dolejš on the calculation of phase diagrams. The latter is also thanked for suggestions on several other issues during the preparation of this manuscript. The authors appreciate the constructive comments and thoughtful suggestions of G. Rebay and an anonymous reviewer, which clearly helped us to improve an earlier version of this work. This manuscript also benefited from reviews of Simon Schorn and another anonymous reviewer. Finally, thanks are also due to D. Robinson and R. White for editorial handling. N. Froitzheim and M. Hauke were supported by the Deutsche Forschungsgemeinschaft (DFG) in the framework of the priority program SPP 2017 "Mountain Building Processes in Four Dimensions (MB-4D)" by grant FR700/21-1.

REFERENCES

Angiboust, S., Agard, P., Jolivet, L., & Beyssac, O. (2009). The Zermatt–Saas ophiolite: The largest (60-km wide) and deepest (c. 70–80 km) continuous slice of oceanic lithosphere detached from a subduction zone? *Terra Nova*, 21, 171–180. https://doi.org/10.1111/j.1365-3121.2009.00870.x

Angiboust, S., Glodny, J., Oncken, O., & Chopin, C. (2014). In search of transient subduction interfaces in the Dent Blanche–Sesia Tectonic System (W. Alps). *Lithos*, 205, 298–321. https://doi.org/10.1016/j.lithos.2014.07.001

Angiboust, S., Yamato, P., Hertgen, S., Hyppolito, T., Bebout, G. E., & Morales, L. (2017). Fluid pathways and high pressure metasomatism in a subducted continental slice (Mt. Emilius klippe, W. Alps). *Journal of Metamorphic Geology*, 35, 471–492. https://doi.org/10.1111/jmg.12241

Ballèvre, M., Kienast, J. R., & Vuichard, J. P. (1986). La "nappe de la Dent Blanche" (Alpine occidentales): Deux unites austroalpines indépéndantes. *Eclogae Geologicae Helvetiae*, 79, 57–74.

Ballèvre, M., & Merle, O. (1993). The Combin Fault: Compressional reactivation of a Late Cretaceouse Early Tertiary detachment fault in the Western Alps. *Schweizerische Mineralogische Und Petrographische Mitteilungen*, 73, 205–227.

Barnicoat, A. C., & Fry, N. (1986). High-pressure metamorphism of the Zermatt–Saas ophiolite zone, Switzerland. *Journal of the Geological Society*, 143, 607–618. https://doi.org/10.1144/gsjgs.143.4.0607

Bearth, P. (1967). Die Ophiolithe der Zone von Zermatt–Saas Fee. Beiträge zur geologischen Karte der Schweiz, N. F., 132, Schweizerischen Geologischen Kommission, Bern.

Beinlich, A., Klemd, R., John, T., & Gao, J. (2010). Trace-element mobilization during Ca-metasomatism along a major fluid conduit: Eclogitization of blueschist as a consequence of fluid–rock interaction. *Geochimica et Cosmochimica Acta*, 74, 1892–1922. https://doi.org/10.1016/j.gca.2009.12.011

Beltrando, M., Rubatto, D., & Manatschal, G. (2010). From passive margins to orogens. The link between ocean–continent transition zones and (ultra-)high-pressure metamorphism. *Geology*, 38, 559–562. https://doi.org/10.1130/G30768.1

Benciolini, L. (1996). Eclogitized websterite-rich subcontinental mantle slice in the austroalpine Mt. Emilius nappe. *Memorie Societa di Geologia Padova*, 48, 73–91.

Bilek, S. L., & Lay, T. (2018). Subduction zone megathrust earthquakes. *Geosphere*, 14, 1468–1500. https://doi.org/10.1130/GES01608.1

Bizzarro, M., Baker, J. A., Haack, H., Ulfbeck, D., & Rosing, M. (2003). Early history of Earth's crust-mantle system inferred from hafnium isotopes in chondrites. *Nature*, 421, 931–933. https://doi.org/10.1038/nature01421

Bocchio, R., Benciolini, L., Martin, S., & Tartarotti, P. (2000). Geochemistry of eclogitised Fe-Ti-gabbros from various lithological settings (Aosta Valley ophiolites, Italian western Alps). Protolith composition and eclogitic paragenesis. *Periodico di Mineralogia*, 69, 217–237.

Bousquet, R., Engi, M., Gosso, G., Oberhänsli, R., Berger, A., Spalla, M., Zucali, M., & Goffè, B. (2004). Explanatory notes to the map: Metamorphic structure of the Alps transition from the Western to the Central Alps. *Mitteilung der Österreichischen Mineralogischen Gesellschaft*, 149, 145–156.

Bovay, T., Lanari, P., Rubatto, D., Smit, M., & Piccoli, F. (2021). Pressure–temperature–time evolution of subducted crust revealed by complex garnet zoning (Theodul Glacier Unit, Switzerland). *Journal of Metamorphic Geology*, 1–32. https://doi.org/10.1111/JMG.12623

Bucher, K., Fazis, Y., de Capitani, C., & Grapes, R. (2005). Blueschists, eclogites, and decompression assemblages of the Zermatt–Saas ophiolite: High-pressure metamorphism of subducted Tethys lithosphere. *American Mineralogist*, 90, 821–835. https://doi.org/10.2138/am.2005.1718

Bucher, K., Weisenberger, T. B., Klemm, O., & Weber, S. (2019). Decoding the complex internal chemical structure of garnet porphyroblasts from the Zermatt area, Western Alps. *Journal of Metamorphic Geology*, 37(9), 1–19. https://doi.org/10.1111/jmg.12506

Bucher, K., Weisenberger, T. B., Weber, S., Klemm, O., & Corfu, F. (2020). The Theodul Glacier Unit, a slab of pre-Alpine rocks in the Alpine meta-ophiolite of Zermatt-Saas, Western Alps. *Swiss Journal of Geosciences*, 113(1), 1–22. https://doi.org/10.1186/s00015-020-00354-6

Coggon, R., & Holland, T. J. B. (2002). Mixing properties of phengitic micas and revised garnet-phengite thermobarometers. *Journal of Metamorphic Geology*, 20, 683–696. https://doi.org/10.1046/j.1525-1314.2002.00395.x

Compagnoni, R. (1977). The Sesia-Lanzo Zone: High pressure-low temperature metamorphism in the Austroalpine continental margin. *Rendiconti Della Società Italiana di Mineralogia e Petrologia*, 33, 335–374.

Dal Piaz, G. V., Cortiana, G., Del Moro, A., Martin, S., Pennacchioni, G., & Tartarotti, P. (2001). Tertiary age and paleostructural inferences of the eclogitic imprint in the Austroalpine outliers and Zermatt-Saas ophiolite, western Alps. *International Journal of Earth Sciences, Geologische Rundschau*, 90, 668–684. https://doi.org/10.1007/s005310000177

Dal Piaz, G. V., Lombardo, B., & Gosso, G. (1983). Metamorphic evolution of the Mt Emilius klippe, Dent Blanche nappe, Western Alps. *American Journal of Science*, 283A, 438–458.

Dal Piaz, G. V., Venturelli, G., Spadea, P., & Di Battistini, G. (1981). Geochemical features of metabasalts and metagabbros from the Piemonte ophiolite nappe, Italian-Western Alps. *Neues Jahrbuch für Mineralogie Abhandlungen*, 142, 248–269.

Dasgupta, R., & Hirschmann, M. M. (2010). The deep carbon cycle and melting in Earth's interior. *Earth and Planetary Science Letters*, 298, 1–13. https://doi.org/10.1016/j.epsl.2010.06.039

de Capitani, C., & Petrakakis, K. (2010). The computation of equilibrium assemblage diagrams with Theriak/Domino software. *American Mineralogist*, 95, 1006–1016. https://doi.org/10.2138/am.2010.3354

Diener, J. F. A., Powell, R., White, R. W., & Holland, T. J. B. (2007). A new thermodynamic model for clino- and orthoamphiboles in the system Na_2O–CaO–FeO–MgO–Al_2O_3–SiO_2–H_2O–O. *Journal of Metamorphic Geology*, 25, 631–656. https://doi.org/10.1111/j.1525-1314.2007.00720.x

Ellero, A., & Loprieno, A. (2018). Nappe stack of Piemonte–Ligurian units south of Aosta Valley: New evidence from Urtier Valley (Western Alps). *Geological Journal*, 53, 1665–1684. https://doi.org/10.1002/gj.2984

Ellis, D. J., & Green, D. H. (1979). An experimental study of the effect of Ca upon garnet-clinopyroxene Fe–Mg exchange equilibria. *Contributions to Mineralogy and Petrology*, 71, 13–22. https://doi.org/10.1007/BF00371878

Engi, M., Giuntoli, F., Lanari, P., Burn, M., Kunz, B., & Bouvier, A.-S. (2018). Pervasive eclogitization due to brittle deformation and rehydration of subducted basement: Effects on continental recycling? *Geochemistry, Geophysics, Geosystems*, 19, 865–881. https://doi.org/10.1002/2017GC007215

Ernst, W. G. (1988). Tectonic history of subduction zones inferred from retrograde blueschist P-T paths. *Geology*, 16, 1081–1084. https://doi.org/10.1130/0091-7613(1988)016<1081:THOSZI>2.3.CO;2

Ernst, W. G., & Dal Piaz, G. V. (1978). Mineral parageneses of eclogitic rocks and related mafic schists of the Piemonte ophiolite nappe, Breuil-St. Jacques area, Italian Western Alps. *American Mineralogist*, 63, 621–640.

Escher, A., Hunziker, J. C., Marthaler, M., Masson, H., Sartori, M., & Steck, A. (1997). Geologic framework and structural evolution of the western Swiss-Italian Alps. In *Deep structure of the Swiss Alps: Results of NRP 20* (Ed. by Pfiffner et al.) (pp. 205–221). Birkhäuser Verlag.

Fassmer, K., Obermüller, G., Nagel, T. J., Kirst, F., Froitzheim, N., Sandmann, S., Miladinova, I., Fonseca, R. O. C., & Münker, C. (2016). High-pressure metamorphic age and significance of eclogite-facies continental fragments associated with oceanic lithosphere in the Western Alps (Etirol-Levaz Slice, Valtournenche, Italy). *Lithos*, 252–253, 145–159. https://doi.org/10.1016/j.lithos.2016.02.019

Gao, J., John, T., Klemd, R., & Xiong, X. (2007). Mobilization of Ti–Nb–Ta during subduction: Evidence from rutile-bearing

dehydration segregations and veins hosted in eclogite, Tianshan, NW China. *Geochimica et Cosmochimica Acta*, 71, 4974–4996. https://doi.org/10.1016/j.gca.2007.07.027

Gao, J., & Klemd, R. (2001). Primary fluids entrapped at blueschist to eclogite transition; evidence from the Tianshan meta-subduction complex in northwestern China. *Contributions to Mineralogy and Petrology*, 142, 1–14. https://doi.org/10.1007/s004100100275

Gosso, G., Messiga, B., Rebay, G., & Spalla, M. I. (2010). Interplay between deformation and metamorphism during eclogitization of amphibolites in the Sesia–Lanzo Zone of the Western Alps. *International Geology Review*, 52, 1193–1219. https://doi.org/10.1080/00206810903529646

Green, E., Holland, T., & Powell, R. (2007). An order-disorder model for omphacitic pyroxenes in the system jadeite-diopside-hedenbergite-acmite, with applications to eclogitic rocks. *American Mineralogist*, 92, 1181–1189. https://doi.org/10.2138/am.2007.2401

Groppo, C., Beltrando, M., & Compagnoni, R. (2009). The P-T path of the ultra-high pressure Lago Di Cignana and adjoining high-pressure meta-ophiolitic units: Insights into the evolution of the subducting Tethyan slab. *Journal of Metamorphic Geology*, 27, 207–231. https://doi.org/10.1111/j.1525-1314.2009.00814.x

Groppo, C., & Castelli, D. (2010). Prograde P-T evolution of a Lawsonite Eclogite from the Monviso meta-ophiolite (Western Alps): Dehydration and redox reactions during subduction of oceanic FeTi-oxide gabbro. *Journal of Petrology*, 51, 2489–2514. https://doi.org/10.1093/petrology/egq065

Hertgen, S., Yamato, P., Morales, L. F. G., & Angiboust, S. (2017). Evidence for brittle deformation events at eclogite-facies P-T conditions (example of the Mt. Emilius klippe, Western Alps). *Tectonophysics*, 706–707, 1–13.

Holland, T. J. B., & Powell, R. (1998). An internally-consistent thermodynamic dataset for phases of petrological interest. *Journal of Metamorphic Geology*, 16, 309–344. https://doi.org/10.1111/j.1525-1314.1998.00140.x

Krogh, E. J. (1988). The garnet-clinopyroxene Fe–Mg geothermometer—A reinterpretation of existing experimental data. *Contributions to Mineralogy and Petrology*, 99, 44–48. https://doi.org/10.1007/BF00399364

Krogh Ravna, E. J., & Terry, M. P. (2004). Geothermobarometry of UHP and HP eclogites and schists—An evaluation of equilibria among garnet–clinopyroxene–kyanite–phengite–coesite/quartz. *Journal of Metamorphic Geology*, 22, 579–592. https://doi.org/10.1111/j.1525-1314.2004.00534.x

Kunz, B. E., Manzotti, P., von Niederhäusern, B., Engi, M., Darling, J. R., Giuntoli, F., & Lanari, P. (2018). Permian high-temperature metamorphism in the Western Alps (NW Italy). *International Journal of Earth Sciences*, 107, 203–229. https://doi.org/10.1007/s00531-017-1485-6

Lagos, M., Scherer, E., Tomaschek, F., Münker, C., Keiter, M., Berndt, J., & Ballhaus, C. (2007). High precision Lu–Hf geochronology of Eocene eclogite-facies rocks from Syros, Cyclades, Greece. *Chemical Geology*, 243, 16–35. https://doi.org/10.1016/j.chemgeo.2007.04.008

Lardeaux, J. M., & Spalla, M. I. (1991). From granulites to eclogites in the Sesia zone (Italian Western Alps): A record of the opening and closure of the Piedmont ocean. *Journal of Metamorphic Geology*, 9, 35–59. https://doi.org/10.1111/j.1525-1314.1991.tb00503.x

Leech, M. L. (2001). Arrested orogenic development: Eclogitization, delamination, and tectonic collapse. *Earth and Planetary Science Letters*, 185, 149–159. https://doi.org/10.1016/S0012-821X(00)00374-5

Li, C., Arndt, N. T., Tang, Q., & Ripley, E. M. (2015). Trace element indiscrimination diagrams. *Lithos*, 232, 76–83. https://doi.org/10.1016/j.lithos.2015.06.022

Li, J.-L., Klemd, R., Gao, J., & Meyer, M. (2012). Coexisting carbonate-bearing eclogite and blueschist in SW Tianshan, China: Petrology and phase equilibria. *Journal of Asian Earth Sciences*, 60, 174–187. https://doi.org/10.1016/j.jseaes.2012.08.015

Li, X.-P., Rahn, M., & Bucher, K. (2004). Serpentinites of the Zermatt–Saas ophiolite complex and their texture evolution. *Journal of Metamorphic Geology*, 22, 159–177. https://doi.org/10.1111/j.1525-1314.2004.00503.x

Liati, A., & Froitzheim, N. (2006). Assessing the Valais ocean, Western Alps: U-Pb SHRIMP zircon geochronology of eclogite in the Balma unit, on top of the Monte Rosa nappe. *European Journal of Mineralogy*, 18, 299–308. https://doi.org/10.1127/0935-1221/2006/0018-0299

Locock, A. J. (2014). An Excel spreadsheet to classify chemical analyses of amphiboles following the IMA 2012 recommendations. *Computers & Geosciences*, 62, 1–11. https://doi.org/10.1016/j.cageo.2013.09.011

Ludwig, K. R. (2008). *Isoplot 3.7, a geochronological toolkit for Microsoft Excel*. Berkeley Geochronology Center Special Publication.

Manzotti, P., Ballèvre, M., & Dal Piaz, G. V. (2017). Continental gabbros in the Dent Blanche Tectonic System (Western Alps): From the pre-Alpine crustal structure of the Adriatic palaeomargin to the geometry of an alleged subduction interface. *Journal of the Geological Society*, 174, 541–556. https://doi.org/10.1144/jgs2016-071

Meda, M., Marotta, A., & Spalla, M. (2010). The role of mantle hydration into the continental crust recycling in the wedge region. *Geological Society, London, Special Publications*, 332, 149–172. https://doi.org/10.1144/SP332.10

Münker, C., Weyer, S., Scherer, E. E., & Mezger, K. (2001). Separation of high field strength elements (Nb, Ta, Zr, Hf) and Lu from rock samples for MC-ICPMS measurements. *Geochemistry Geophysics Geosystems*, 2, 2001GC000183.

Negro, F., Bousquet, R., Vils, F., Pellet, C.-M., & Hänggi-Schaub, J. (2013). Thermal structure and metamorphic evolution of the Piemont-Ligurian metasediments in the northern Western Alps. *Swiss Journal of Geoscience*, 106, 63–78. https://doi.org/10.1007/s00015-013-0119-7

Oberhänsli, R., & Goffé, B. (2004). Explanatory notes to the map: Metamorphic structure of Alps, introduction. *Mitteilungen der Österreichischen Geologischen Gesellschaft*, 149, 115–123.

Peacock, S. M. (1990). Fluid processes in subduction zones. *Science*, 248, 329–337. https://doi.org/10.1126/science.248.4953.329

Peacock, S. M., & Hyndman, R. D. (1999). Hydrous minerals in the mantle wedge and maximum depth of subduction thrust earthquakes. *Geophysical Reasearch Letters*, 26, 2517–2520. https://doi.org/10.1029/1999GL900558

Pearce, J. A., & Cann, J. R. (1973). Tectonic setting of basic volcanic rocks determined using trace element analyses. *Earth and Planetary Science Letters*, 19, 290–300. https://doi.org/10.1016/0012-821X(73)90129-5

Pennacchioni, G. (1996). Progressive eclogitization under fluid-present conditions of pre-Alpine mafic granulites in the Austroalpine Mt Emilius Klippe (Italian Western Alps). *Journal of Structural Geology*, 18, 549–561. https://doi.org/10.1016/S0191-8141(96)80023-X

Pfeifer, H. R., Colombi, A., & Ganguin, J. (1989). Zermatt–Saas and Antrona Zone: A petrographic and geochemical comparison of polyphase metamorphic ophiolites of the West-Central Alps. *Schweizerische Mineralogische Und Petrographische Mitteilungen*, 69, 217–236.

Philippot, P., & Selverstone, J. (1991). Trace element-rich brines in eclogitic veins: Implications for fluid composition and transport during subduction. *Contributions to Mineralogy and Petrology*, 106, 417–430. https://doi.org/10.1007/BF00321985

Pleuger, J., Roller, S., Walter, J. M., Jansen, E., & Froitzheim, N. (2007). Structural evolution of the contact between two Penninic nappes (Zermatt-Saas zone and Combin zone, Western Alps) and implications for the exhumation mechanism and palaeogeography. *International Journal of Earth Sciences*, 96, 229–252. https://doi.org/10.1007/s00531-006-0106-6

Pognante, U. (1991). Petrological constraints on the eclogite- and blueschist-facies metamorphism and P-T-t paths in the Western Alps. *Journal of Metamorphic Geology*, 9, 5–17. https://doi.org/10.1111/j.1525-1314.1991.tb00501.x

Powell, R. (1985). Regression diagnostics and robust regression in geothermometer/geobarometer calibration: The garnet-clinopyroxene geothermometer revisited. *Journal of Metamorphic Geology*, 2, 33–42. https://doi.org/10.1111/j.1525-1314.1984.tb00283.x

Ranero, C. R., Grevemeyer, I., Sahling, H., Barckhausen, U., Hensen, C., Wallmann, K., Weinrebe, W., Vannucchi, P., von Huene, R., & McIntosh, K. (2008). Hydrogeological system of erosional convergent margins and its influence on tectonics and interplate seismogenesis. *Geochemistry Geophysics Geosystems*, 9, Q03S04. https://doi.org/10.1029/2007GC001679

Rebay, G., Powell, R., & Diener, J. F. A. (2010). Calculated phase equilibria for a MORB composition in a P–T range, 450–650°C and 18–28 kbar: The stability of eclogite. *Journal of Metamorphic Geology*, 28, 635–645. https://doi.org/10.1111/j.1525-1314.2010.00882.x

Rebay, G., Spalla, M. I., & Zanoni, D. (2012). Interaction of deformation and metamorphism during subduction and exhumation of hydrated oceanic mantle: Insights from the Western Alps. *Journal of Metamorphic Geology*, 30, 687–702. https://doi.org/10.1111/j.1525-1314.2012.00990.x

Rebay, G., Zanoni, D., Langone, A., Luoni, P., Tiepolo, M., & Spalla, M. I. (2018). Dating of ultramafic rocks from the Western Alps ophiolites discloses Late Cretaceous subduction ages in the Zermatt-Saas Zone. *Geological Magazine*, 155, 298–315. https://doi.org/10.1017/S0016756817000334

Reddy, S. M., Wheeler, J., & Cliff, R. A. (1999). The geometry and timing of orogenic extension: An example from the Western Italian Alps. *Journal of Metamorphic Geology*, 17, 573–589. https://doi.org/10.1046/j.1525-1314.1999.00220.x

Reinecke, T. (1991). Very-high-pressure metamorphism and uplift of coesite-bearing metasediments from the Zermatt-Saas zone, Western Alps. *European Journal of Mineralogy*, 3, 7–17. https://doi.org/10.1127/ejm/3/1/0007

Reynard, B. (2016). Mantle hydration and Cl-rich fluids in the subduction forearc. *Progress in Earth and Planetary Science*, 3, 9. https://doi.org/10.1186/s40645-016-0090-9

Roda, M., Spalla, M. I., & Marotta, A. M. (2012). Integration of natural data within a numerical model of ablative subduction: A possible interpretation for the Alpine dynamics of the Austroalpine crust. *Journal of Metamorphic Geology*, 30, 973–996. https://doi.org/10.1111/jmg.12000

Rosenbaum, G., & Lister, G. S. (2005). The Western Alps from the Jurassic to Oligocene: Spatio-temporal constraints and evolutionary reconstructions. *Earth Science Reviews*, 69, 281–306. https://doi.org/10.1016/j.earscirev.2004.10.001

Rubatto, D., Gebauer, D., & Compagnoni, R. (1999). Dating of eclogite-facies zircons: The age of Alpine metamorphism in the Sesia-Lanzo Zone (Western Alps). *Earth and Planetary Science Letters*, 167, 141–158. https://doi.org/10.1016/S0012-821X(99)00031-X

Rubatto, D., Gebauer, D., & Fanning, M. (1998). The youngest basic oceanic magmatism in the Alps (Late Cretaceous; Chiavenna unit, Central Alps): Geochronological constraints and geodynamic significance. *Contribution of Mineralogy and Petrology*, 132, 269–287. https://doi.org/10.1007/s004100050421

Scambelluri, M., Pennacchioni, G., Gilio, M., Bestmann, M., Plümper, O., & Nestola, F. (2017). Fossil intermediate-depth earthquakes in subducting slabs linked to differential stress release. *Nature Geoscience*, 10, 960–966. https://doi.org/10.1038/s41561-017-0010-7

Scambelluri, M., Pennacchioni, G., & Philippot, P. (1998). Salt-rich aqueous fluids formed during eclogitization of metabasites in the Alpine continental crust (Austroalpine Mt. Emilius unit, Italian western Alps). *Lithos*, 43, 151–167. https://doi.org/10.1016/S0024-4937(98)00011-5

Scherer, E. E., Mezger, K., & Münker, C. (2003). The ^{176}Lu decay constant discrepancy: Terrestrial samples vs. meteorites. *Meteorites and Planetary Science Supplement*, 38, A136.

Scherer, E. E., Münker, C., & Mezger, K. (2001). Calibration of the lutetium–hafnium clock. *Science*, 293, 683–687. https://doi.org/10.1126/science.1061372

Schmid, S. M., Fügenschuh, B., Kissling, E., & Schuster, R. (2004). Tectonic map and overall architecture of the Alpine orogen. *Eclogae Geologicae Helvetiae*, 97, 93–117. https://doi.org/10.1007/s00015-004-1113-x

Skora, S., Mahlen, N. J., Johnson, C. M., Baumgartner, L. P., Lapen, T. J., Beard, B. L., & Szilvagyi, E. T. (2015). Evidence for protracted prograde metamorphism followed by rapid exhumation of the Zermatt-Saas Fee ophiolite. *Journal of Metamorphic Geology*, 33, 711–734. https://doi.org/10.1111/jmg.12148

Söderlund, U., Patchett, P. J., Vervoort, J. D., & Isachsen, C. E. (2004). The ^{176}Lu decay constant determined by Lu–Hf and U–Pb isotope systematics of Precambrian mafic intrusions. *Earth and Planetary Science Letters*, 219, 311–324. https://doi.org/10.1016/S0012-821X(04)00012-3

Stampfli, G. M., Mosar, J., Marquer, D., Marchant, R., Baudin, T., & Borel, G. (1998). Subduction and obduction processes in the

western Alps. *Tectonophysics*, 296, 159–204. https://doi.org/10.1016/S0040-1951(98)00142-5

Steck, A., Masson, H., & Robyr, M. (2015). Tectonics of the Monte Rosa and surrounding nappes (Switzerland and Italy): Tertiary phases of subduction, thrusting and folding in the Pennine Alps. *Swiss Journal of Geoscience*, 108, 3–34. https://doi.org/10.1007/s00015-015-0188-x

van der Straaten, F., Schenk, V., John, T., & Gao, J. (2008). Blueschist-facies rehydration of eclogites, Tian Shan, NW-China: Implications for fluid–rock interaction in the subduction channel. *Chemical Geology*, 255, 195–219. https://doi.org/10.1016/j.chemgeo.2008.06.037

Vervoort, J. D., Patchett, P. J., Söderlund, U., & Baker, M. (2004). Isotopic composition of Yb and the determination of Lu concentrations and Lu/Hf ratios by isotope dilution using MC-ICPMS. *Geochemistry Geophysics Geosystems*, 5, Q11002. https://doi.org/10.1029/2004GC000721

Vitale Brovarone, A., Groppo, C., Hetényi, G., Compagnoni, R., & Malavieille, J. (2011). Coexistence of lawsonite-bearing eclogite and blueschist: Phase equilibria modelling of Alpine Corsica metabasalts and petrological evolution of subducting slabs. *Journal of Metamorphic Geology*, 29, 583–600. https://doi.org/10.1111/j.1525-1314.2011.00931.x

Weber, S., & Bucher, K. (2015). An eclogite-bearing continental tectonic slice in the Zermatt– Saas high-pressure ophiolites at Trockener Steg (Zermatt, Swiss Western Alps). *Lithos*, 232, 336–359. https://doi.org/10.1016/j.lithos.2015.07.010

Weber, S., Sandmann, S., Miladinova, I., Fonseca, R. O. C., Froitzheim, N., Münker, C., & Bucher, K. (2015). Dating the initiation of Piemonte–Liguria Ocean Subduction: Lu–Hf garnet chronometry of eclogites from the Theodul Glacier Unit (Zermatt–Saas Zone, Switzerland). *Swiss Journal of Geoscience*, 108, 183–199. https://doi.org/10.1007/s00015-015-0180-5

Wei, C. J., & Clarke, G. L. (2011). Calculated phase equilibria for MORB compositions: A reappraisal of the metamorphic evolution of lawsonite eclogite. *Journal of Metamorphic Geology*, 29, 939–952. https://doi.org/10.1111/j.1525-1314.2011.00948.x

White, R. W., Powell, R., & Holland, T. J. B. (2007). Progress relating to calculation of partial melting equilibria for metapelites. *Journal of Metamorphic Geology*, 25, 511–527. https://doi.org/10.1111/j.1525-1314.2007.00711.x

Widmer, T., & Thompson, A. B. (2001). Local origin of high pressure vein material in eclogite facies rocks of the Zermatt-Saas zone, Switzerland. *American Journal of Science*, 301, 627–656. https://doi.org/10.2475/ajs.301.7.627

Zack, T., & John, T. (2007). An evaluation of reactive fluid flow and trace element mobility in subducting slabs. *Chemical Geology*, 239, 199–216. https://doi.org/10.1016/j.chemgeo.2006.10.020

Zanoni, D., Rebay, G., & Spalla, M. I. (2016). Ocean floor and subduction record in the Zermatt- Saas rodingites, Valtournanche, Western Alps. *Journal of Metamorphic Geology*, 34, 941–961. https://doi.org/10.1111/jmg.12215

SUPPORTING INFORMATION

Additional supporting information may be found in the online version of the article at the publisher's website.

Figure S1: (a-b) *P–T* pseudosection for the representative eclogite assemblage of sample SW108 calculated with $X_{Fe^{3+}} = 0.1$ and 0.2 in (a) and (b) respectively. The modelling approach is the same as described in caption to Figure 12.

Figure S2: (a-b) *P–T* pseudosection for the representative eclogite assemblage of sample SW114 calculated with $X_{Fe^{3+}} = 0.1$ and 0.2 in (a) and (b) respectively. The modelling approach is the same as described in caption to Figure 12.

Figure S3: (a-b) *P–T* pseudosection for the representative blueschist of sample SW133 calculated with $X_{Fe^{3+}} = 0.1$ and 0.2 in (a) and (b) respectively. The modelling approach is the same as described in caption to Figure 13.

Figure S4: (a-b) *P–T* pseudosection for the representative blueschist of sample SW135 calculated with $X_{Fe^{3+}} = 0.1$ and 0.2 in (a) and (b) respectively. The modelling approach is the same as described in caption to Figure 13.

How to cite this article: Weber, S., Hauke, M., Martinez, R.E., Redler, C., Münker, C. & Froitzheim, N. (2022) Fluid-driven transformation of blueschist to vein eclogite during the Early Eocene in a subducted sliver of continental crust (Monte Emilius, Italian Western Alps). *Journal of Metamorphic Geology*, 40(3), 553–584. Available from: https://doi.org/10.1111/jmg.12638